SUPPORTING INFORMATION

Controlling conjugated polymer morphology by precise oxygen position in single-ether side chains

Pablo Durand,[a] Huiyan Zeng,[b] Badr Jismy,[a] Olivier Boyron,[c] Benoît Heinrich,[d] Laurent Herrmann,[b] Olivier Bardagot,*[a] Ioannis Moutsios,[e] Alina V. Mariasevskaia,[f] Alexey P. Melnikov,[f] Dimitri A. Ivanov,[e,f] Martin Brinkmann*[b] and Nicolas Leclerc*[a]

[a] Université de Strasbourg, CNRS, ICPEES UMR 7515, F-67087 Strasbourg, France

[b] Université de Strasbourg, CNRS, ICS UPR 22, F-67000 Strasbourg, France

[c] Université de Lyon, CNRS, Laboratoire CP2M, UMR 5128, 69100 Villeurbanne, France

[d] Université de Strasbourg, CNRS, IPCMS UMR 7504, F-67034 Strasbourg, France

[e] Université de Mulhouse, CNRS, IS2M, UMR 7361, F-68057 Mulhouse, France

[f] Faculty of Chemistry, Lomonosov Moscow State University, GSP-1, 1-3 Leninskiye Gory, 119991 Moscow, Russia

Table of contents

Materials and methods.

NMR analysis. ^{1}H, ^{13}C NMR NMR spectra were recorded on a Bruker 400 UltrashieldTM 400 MHz NMR spectrometer, with an internal lock on the ^{2}H-signal of the solvent ($CDCl_3$).

Size exclusion chromatography. Size Exclusion Chromatography (**SEC**) measurements were performed with Viscotek system, from Malvern Instruments, that incorporates a differential refractive index, a dual light-scattering detector and a viscosimeter. 1,2,4-Trichlorobenzene was used as the mobile phase at a flow rate of 1 mL/min at 150°C. It was stabilized with 2,6-di(*tert*-butyl)-4-methylphenol (200 mg L^{-1}). The polymer was injected at a concentration of 1 mg/mL. The separation was carried out on three Agilent columns (PLgel Olexis from Agilent Technologies, 300 mm × 7.5 mm, 13µm) protected by a guard column (PL gel 5 µm). Columns and detectors were maintained at 150°C. The OmniSEC software version 5.2 was used for data acquisition and analysis. The molar mass distributions were calculated with a calibration curve based on narrow polystyrene standards (Polymer Standard Service, Mainz), using only the refractometer detector.

Thermal properties. TGA measurements were performed with TA Instruments Q50 from instrument, operated under nitrogen at scan rate of 5 ^{o}C/min.

DSC measurements were performed with TA Instruments Q1000 instrument, operated under nitrogen at scan rate of 5 ^{o}C/min on heating and on cooling. Endotherm up.

Fast scanning chip calorimetry or nanocalorimetry measurements were performed on a commercial fast scanning calorimeter, Flash DSC 2+ (made by Mettler-Toledo, Switzerland) equipped with an intracooler. Prior to experiments, each sensor (Multistar UFS 1) was conditioned and calibrated. A purge of nitrogen gas was used to provide an inert atmosphere with the constant flow rate 50 mL/min. To erase the structural memory of the samples, they were preliminarily heated at a rate of 1000 K/s to 325 °C for 100 ms and then immediately cooled down at the same rate. Endotherm up.

Cyclic voltammetry. Oxidation and reduction potentials were determined by cyclic voltammetry with a conventional 3-electrode system using a BioLogic potentiostat equipped with a platinum micro disk (2 mm^2) working electrode and a platinum wire counter electrode. Potentials were calibrated versus the saturated calomel electrode (SCE) at a conventional scan rate of 100 mV/s. Recrystallized tetrabutylammonium hexafluorophosphate (Bu_4NPF_6) was used as the supporting electrolyte (0.1 M) in distilled and anhydrous acetonitrile. Acetonitrile was distilled from CaH2 under a nitrogen atmosphere. The ferrocene/ferrocenium couple was used as an internal reference.

Orientation and doping of thin films. Anhydrous solvents (99%) used for doping (acetonitrile and nitromethane) and film preparation (ortho-dichlorobenzene) (NaPSS) were purchased from Sigma Aldrich as well as Sodium Poly(styrene sulfonate). The orientation of the films by high-Temperature rubbing followed the protocol described in previous publications.[S1-S3] First, a thin PBTTT film was deposited by doctor blading at 156 °C a solution at 10 g/L in ODCB onto clean microscope glass slides coated with a thin NaPSS sacrificial layer (spin-coated at 3000 rpm using a 10 g/L aqueous solution of NaPSS). Microscope glass slides were cleaned by sonication (15 min per step) in acetone, ethanol, a 5% aqueous Hellmanex solution and finally three rinsing steps in distilled water. Rubbing is performed by using a homemade set-up consisting of a rotating cylinder (rotation speed of 600 rpm) covered with a microfiber cloth and a translating hot plate (1 mm/s). The film thickness was extracted from the UV-vis absorbance using the calibration given in reference S4.

The doping of the PBTTT films with F_6TCNNQ was performed following the incremental concentration doping (ICD) procedure with full sample immersion for 40 sec in the dopant solution of increasing concentration from 0.05 to 5 $mg.ml^{-1}$.[S2] The doped films were not rinsed with the pure solvent to avoid de-doping of the films. Both doping and rubbing were performed in a Jacomex glovebox.

Absorption spectroscopy. Standard absorption spectra were recorded on Shimadzu UV-1800 model spectrophotometer. In solid state, the absorption spectra were measured on thin films spin-coated on glass substrates from a 0.5 mg/mL chlorobenzene solution.

For polarized UV–Vis–NIR absorption, a Varian Cary 5000 spectrometer with polarized incident light and spectral resolution of 1 nm has been used on the doped films (350–2500 nm). For all polarized UV-Vis-NIR measurements, the PBTTT/NaPSS/glass films are used without floating. The film thickness was in the range 55-60 nm. Alignment of pristine and doped polymer films was quantified by the dichroic ratio (DR) and the 3D order parameter (OP) following the equations:

$$DR = \frac{Abs//}{Abs_{\perp}} \quad (2)$$

$$OP = \frac{DR - 1}{DR + 2} \quad (3)$$

Where $Abs_{//}$ is the absorption parallel to the rubbing and $Abs_{\perp}$ is the absorption perpendicular to the rubbing direction.

Synchrotron micro-focus SAXS and WAXS. These experiments were conducted in situ on nanocalorimetric sensors using a custom-built nanocalorimetric device described previously. To perform crystallization from melt of a few nanogram-size PBTTT samples, small fragments (1-2 mm^2) of all PBTTT polymer thin films were cut into square 50x50 μm^2 pieces using a razor blade. Square pieces were placed in the center of the active area (100x100 μm^2) of commercially available nanocalorimetric sensors XEN-39392 (Xensor Integration). After a short annealing time at 250 °C (less than 1 s), the samples were subjected to isothermal crystallization at 40 °C directly on the nanocalorimetric sensors for 2 days for the samples with faster crystallization kinetics (PBTTT-^{11}O, PBTTT-^{8}O) and for 5 days for the samples with slower kinetics (PBTTT-^{5}O, PBTTT-^{3}O).

The X-ray micro-diffraction experiments were performed at the microfocus extension of beamline ID13 at the European Synchrotron Radiation Facility (ESRF, Grenoble, France). X-rays with a photon energy of 13 keV were focused with beryllium lenses arranged in a vacuum transfocator

placed in the EH2 44m downstream the undulator source. The typical beam spot size was estimated to be around 10 × 15 microns. A single photon counting pixel array detector (Eiger 4M) from Dectris was placed 46 cm behind the sample, perpendicular to the X-ray path. The samples were mounted in transmission geometry. 2D diffraction patterns were taken from a two-dimensional scanning of the sample with a 10 μm step for both horizontal and vertical directions of mesh scan. The norm of the scattering vector **q** ($|s| = 4\pi \sin(\theta)/\lambda$, where θ is the Bragg angle and λ- the wavelength), corresponding to the detector pixel array was calibrated with several diffraction peaks of silver behenate. The acquired data was reduced and corrected using pyFAI package. The data analysis and visualization were done using home build routines developed in the Igor Pro software package (Wavemetrics) and Python 3.8.

Transmission Electron Microscopy. Oriented areas of both polymers were identified for TEM analysis by optical microscopy (Leica DMR-X microscope). For TEM investigations, the oriented PBTTT thin films prepared on NaPSS by high temperature rubbing were carbon-coated and the films were recovered on copper TEM grids by floating on water. The TEM grids were doped by ICD using F_6TCNNQ solutions in acetonitrile inside the glove box and rapidly transferred to the TEM for measurements. For experiments *versus* dopant concentration, the samples were left for 1 min in the solutions. The structural variation in the doped thin films was followed by electron diffraction using a transmission electron microscope. In the case of ICD, the grids were doped by dipping in solutions of increasing concentration up to the desired concentration.[S2] TEM was performed in bright field and diffraction modes using a CM12 Philips microscope equipped with a MVIII (Soft Imaging System) charge coupled device camera. Calibration of the reticular distances in the ED patterns was made with an oriented polytetrafluoroethylene (PTFE) film. As an alternative, the (003) reflection of PBTTT was used as a reference (4.55 Å). Beam exposure was set to a minimum using the low dose system to avoid de-doping under the electron beam that is observed when the same zone is exposed for a prolonged period of time.

Charge conductivity and Seebeck coefficient. The detailed device preparation method is described in reference S3. All devices were fabricated on glass substrates, cleaned by ultrasonication in acetone, ethanol, Hellmanex and deionized water (x3 times). The cleaned substrates were dried under nitrogen and exposed to plasma prior to film deposition. Gold electrical contacts (40 nm thick) in a four-points probe geometry (1 mm spacing between electrodes, 5 mm length) were evaporated through a shadow mask (rate of 4–6 Å/s) after deposition of a first layer of chromium (2.5 nm thick) (evaporation rate 0.5–1 Å/s).

The geometry of deposited gold electrodes allows determining the charge transport and thermopower on a same substrate in both parallel and perpendicular directions to rubbing (see support in figures in reference S3). Oriented films of PBTTT-^{x}O were floated on distilled water and carefully recovered on the device with pre-deposited gold electrodes. After float-off, the samples are left for drying 1hr in ambient and then transferred in the glovebox via the transfer chamber under primary vacuum (pumping for several minutes). Doping using incremental concentration doping (ICD) methods were performed on the polymer/device samples in a glovebox (Jacomex). ICD involves immersing the sample for 40 s in dopant solutions of increasing concentration following the sequence: 0.05, 0.1, 0.5, 1, 2 and 5 mg.mL^{-1}. Four-point probe measurements of electrical conductivity were performed using a Keithley 4200-SCS and a Lab Assistant Semiprobe station under N_2 atmosphere. To derive the resistivity ρ from the sheet resistance R measured on the device, the geometrical correction factor C was first determined such that ρ = R.C.t where t is the film thickness. The geometrical correction factor C was determined for four-line electrode geometry by measuring the sheet resistance on the same sample using a classical four-point apparatus and the four-line electrode device, yielding C = 1.81. The average conductivity value for a given rubbing temperature was taken as the average of two to four devices.

Thermopower measurements were conducted in nitrogen atmosphere on the same devices. The thermopower was measured using a differential temperature method whereby a temperature gradient is established across the sample along or perpendicular to the rubbing direction. The details of the experimental setup are given in reference S3.

Synthesis

The PBTTT-C_{12} synthesis has been already reported in reference S4.

The PBTTT-^{8}O has been synthesized following the chemical route described in Scheme S1.

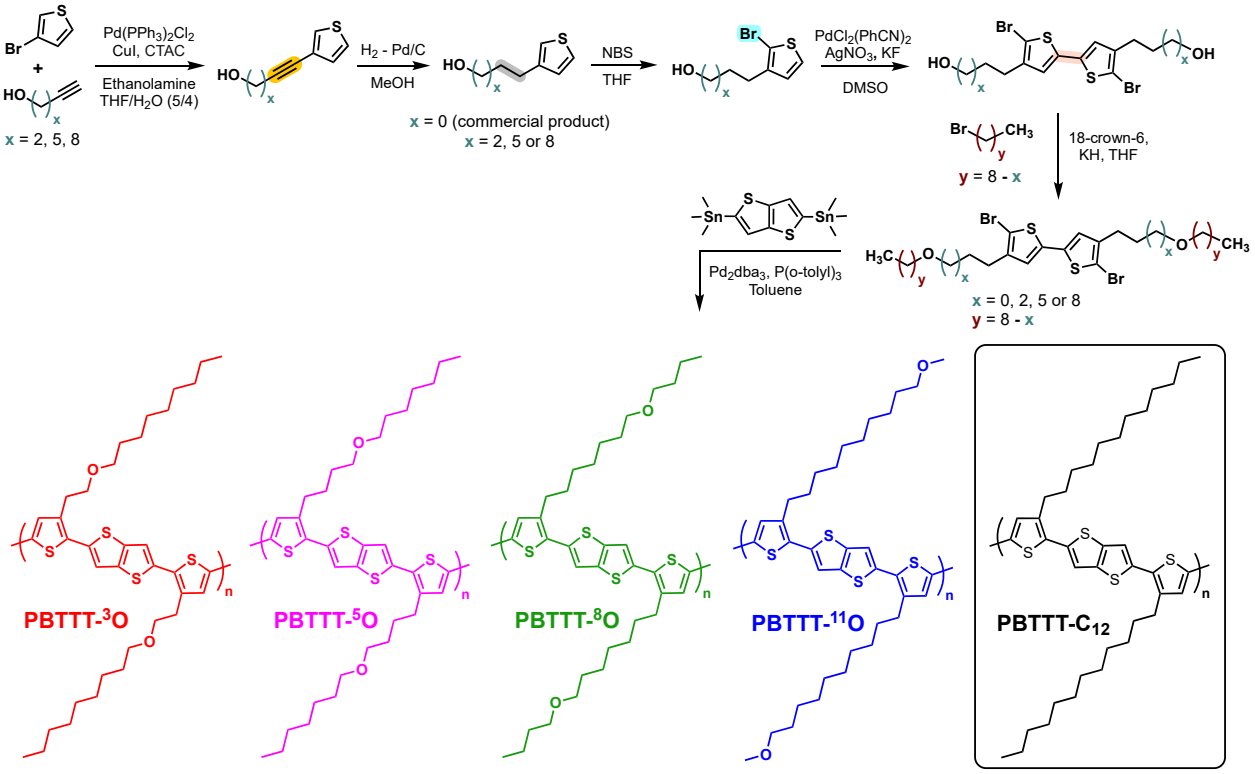

Scheme S1. General synthetic route towards the ether-based PBTTTs, applied here to the synthesis of the PBTTT-^{11}O. PBTTT-^{3}O, PBTTT-^{5}O, PBTTT-^{8}O, PBTTT-^{11}O and PBTTT-C_{12} polymer structures.

General procedure 1: Sonogashira coupling

To a 2 L RBF equipped with a magnetic stirring bar were added the corresponding alkyne (100 mmol), 3-bromothiophene (14.1 mL, 150 mmol), hexadecyltrimethylammonium chloride (3.2 g, 10 mmol), ethanolamine (12 mL, 200 mmol), THF (500 mL) and water (400 mL). The mixture was degassed with 3 vacuum / argon cycle. Then were added $PdCl_2(PPh_3)_2$ (3.5 g, 5 mmol) and CuI (1.9 g, 10 mmol). The mixture was degassed again and stirred for 24 h at 60 °C. The mixture was extracted with EtOAc, washed with brine and solvent removed under vacuum. The oily residue

was purified by flash chromatography twice (PE to PE:EtOAc 20 %) and (PE to DCM) to afford the product as a colorless oil.

General procedure 2: Alkyne reduction

To a 250 mL RBF equipped with a magnetic stirring bar were added the product from the previous reaction (90 mmol), 10wt% Pd/C (2 g, 1.89 mmol) and MeOH (150 mL). The mixture was stirred at room temperature under hydrogen atmosphere. The extent of reaction was followed by ^{1}H NMR spectroscopy. At the end of the reaction the mixture was filtered on a fritted funnel and solvent removed under vacuum leaving a colorless oil which was used in the next step without further purification.

General procedure 3: Bromination

An ice cooled 250 mL flask equipped with a magnetic stirring bar was filled with the product from the previous reaction (22.7 mmol) and THF (150 mL). The flask was chilled 10 min and NBS (4.24 g, 23.8 mmol) was slowly added. The reaction was stirred and allowed to reach room temperature overnight. The reaction was then extracted with EtOAc and washed with 3 M NaOH, water and brine and then concentrated under vacuum. The oily residue was purified twice by flash chromatography (PE to PE:EtOAc 20 %) and (PE to DCM) to give the product as a colorless oil.

General procedure 4: Homocoupling

In a 250 mL flask equipped with a magnetic stir bar was added the product from procedure 3 (11.5 mmol), KF (1.34 g, 23 mmol), $AgNO_3$ (3.92 g, 23 mmol), $PdCl_2(PhCN)_2$ (44 mg, 0.12 mmol) and DMSO (80 mL). The mixture was stirred and degassed with 3 vacuum argon cycles and heated to 60 °C for 3 h. Then was added again KF (1.34 g, 23 mmol) and $AgNO_3$ (3.92 g, 23 mmol) and the reaction was continued overnight. Then was added H_2O (100 mL) and the mixture was extracted with Et_2O, washed with H_2O, brine and solvent removed under vacuum. The oily residue was

purified by flash chromatography (PE to PE:EtOAc 40 %) to give a yellow solid. Two recrystallizations in the appropriate solvent afforded the pure product as pale-yellow solid.

General procedure 5: Side chain termination

In a flame dried 25 mL flask equipped with a magnetic stir bar was added the product from procedure 4 (1 mmol), the appropriate n-alkyl bromide/iodide (20 mmol), 18-crown-6 (53 mg, 0.2 mmol), and dry THF (12 mL). The flask was capped with a septum and evacuated with argon. The mixture was stirred on ice bath then was added KH 30 % in mineral oil (0.53 g, 4 mmol) and allowed to reach room temperature. After completion (TLC check) the reaction was diluted in H_2O and extracted with Et_2O, washed with H_2O, brine and solvent removed under vacuum. The oily residue was purified twice by flash chromatography (PE to PE:EtOAc 5 %).

General procedure 6: Polymerization

In a 100 mL Schlenck flask was added, monomer 1 (1 eq), monomer 2 (1 eq), P(*o*-tolyl)$_3$ (0.08 eq) and toluene (90 mL / 1 mmol). The solution was degased with an argon stream and $Pd_2(dba)_3$ (0.02 eq) was added. The flask was then capped and the solution stirred at 120 °C for 24h.

Then the polymer chains were end capped. First, 2-bromothiophène (0.1 eq) was added and the solution was stirred at 120 °C. After 30 min, 2-(trimethylstannyl)thiophene (0.1 eq) was then added and the solution was stirred for another 30 min at 120 °C.

The reaction was then quenched by pouring the polymer solution into absolute ethanol. The polymer was filtered into a Soxhlet extraction cartridge. The polymer was purified by Soxhlet extraction with acetone, cyclohexane and chlorobenzene. Acetone and cyclohexane fraction were discarded and the chlorobenzene fraction treated with 100 mL of saturated diethyldithiocarbamate solution at 60 °C for 1 h. The organic layer was then washed several times with deionized water and the solvent were removed under vacuum. The polymer was taken off the flask using a spatula and EtOH, it was then filtered on a Teflon membrane and dried under vacuum.

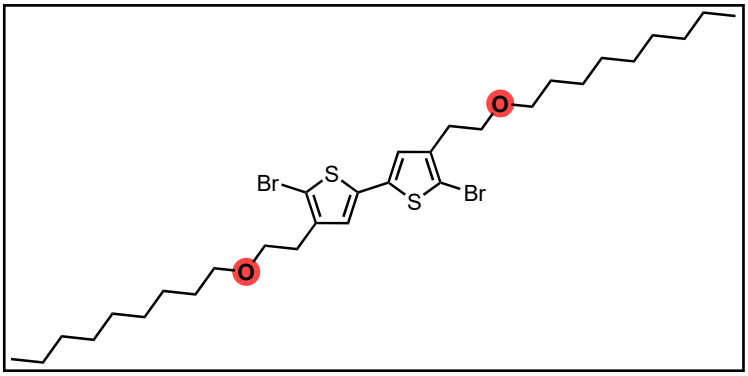

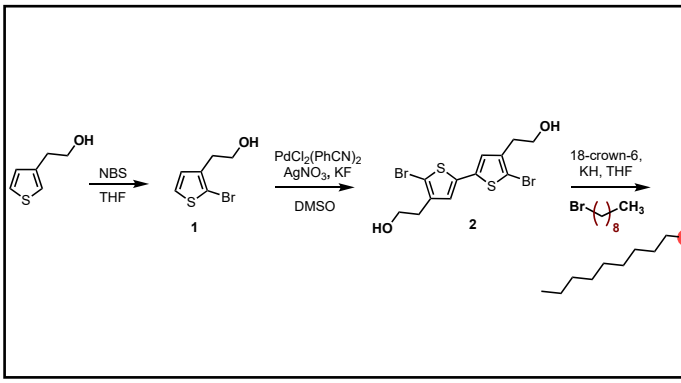

Scheme S2. Synthetic route towards the PBTTT-^{3}O.

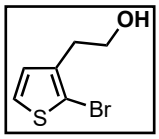

2-(2-bromothiophen-3-yl)ethan-1-ol (1): General procedure 2 was applied to the commercially available 2-(thiophen-3-yl)ethan-1-ol. Yield = 68%

^{1}H NMR ($CDCl_3$, 400MHz) δ: 7.23 (d, 1H, J=5.6Hz), 6.87 (d, 1H, J=5.6Hz), 3.83 (t, 2H, J=6.6Hz), 2.86 (t, 2H, J=6.6Hz), 1.70 (s, 1H)

^{13}C NMR ($CDCl_3$, 400MHz) δ: 138.08, 128.67, 125.83, 110.48, 62.19, 32.91

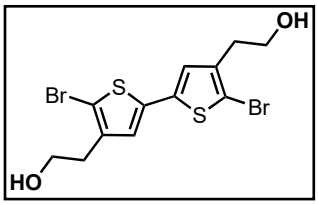

2,2'-(5,5'-dibromo-[2,2'-bithiophene]-4,4'-diyl)bis(ethan-1-ol) (2): General procedure 4 was applied to compound (1). Recrystallized twice in chloroform. Yield = 58%

^{1}H NMR ($CDCl_3$, 400MHz) δ: 6.87 (s, 2H), 3.86 (t, 4H, J=6.5Hz), 2.83 (t, 4H, J=6.5Hz), 1.48 (bs, 2H)

^{13}C NMR ($(CD_3)_2CO$), 400MHz) δ: 141.65, 136.66, 126.56, 109.07, 61.63, 33.84

5,5'-dibromo-4,4'-bis(2-(nonyloxy)ethyl)-2,2'-bithiophene (3): General procedure 5 was applied to compound (2) with 1-bromononane. Yield = 77%

^{1}H NMR ($CDCl_3$, 400MHz) δ: 6.86 (s, 2H), 3.59 (t, 4H, J=6.8Hz), 3.44 (t, 4H, J=6.6Hz), 2.81 (t, 4H, J=6.9Hz), 1.56 (m, 4H), 1.38-1.21 (m, 24H), 0.88 (t, 6H, J=6.9Hz)

^{13}C NMR ($CDCl_3$, 400MHz) δ: 139.74, 136.28, 125.15, 109.03, 71.26, 69.63, 32.04, 30.29, 29.89, 29.74, 29.67, 29.45, 26.39, 22.83, 14.27

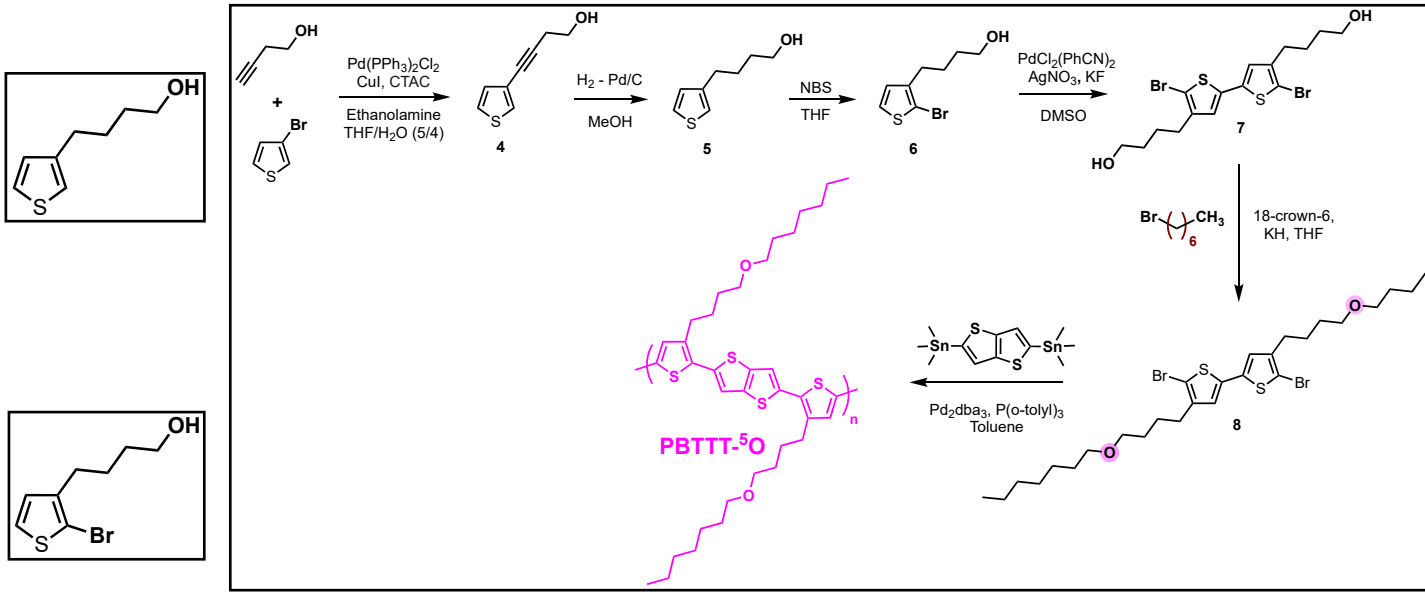

Scheme S3. Synthetic route towards the PBTTT-^{5}O.

4-(thiophen-3-yl)but-3-yn-1-ol (4): General procedure 1 was applied to butyn-1-ol with 3-bromothiophene. Yield = 82%

^{1}H NMR ($CDCl_3$, 400MHz) δ: 7.38 (dd, 1H, J_1=3.1Hz, J_2=1.2Hz), 7.23 (dd, 1H, J_1=5.0Hz, J_2=3.0Hz), 7.08 (dd, 1H, J_1=5.0Hz, J_2=1.2Hz), 3.78 (t, 2H, J=6.3Hz), 2.65 (t, 2H, J=6.3Hz), 2.26 (bs, 1H)

^{13}C NMR ($CDCl_3$, 400MHz) δ: 130.01, 128.33, 125.26, 122.37, 86.13, 77.52, 61.15, 23.82

4-(thiophen-3-yl)butan-1-ol (5): General procedure 2 was applied to compound (4). Yield = 88%

^{1}H NMR ($CDCl_3$, 400MHz) δ: 7.24 (m, 1H), 6.94 (m, 2H), 3.67 (td, 2H, J_1=6.3Hz, J_2=6.3Hz), 2.67 (t, 2H, J=7.3Hz), 1.71 (m, 2H), 1.62 (m, 2H), 1.23 (bs, 1H)

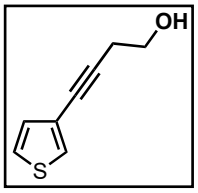

^{13}C NMR ($CDCl_3$, 400MHz) δ: 142.7, 128.2, 125.3, 120.0, 62.8, 32.4, 30.0, 26.7

4-(2-bromothiophen-3-yl)butan-1-ol (6): General procedure 3 was applied to compound (5). Yield = 91%

^{1}H NMR ($CDCl_3$, 400MHz) δ: 7.19 (d, 1H, J=5.6Hz), 6.80 (d, 1H, J= 5.6Hz), 3.67 (t, 2H, J=6.4Hz), 2.61 (t, 2H, J=7.4Hz), 1.70-1.58 (m, 4H), 1.45 (bs, 1H)

^{13}C NMR ($CDCl_3$, 400MHz) δ: 141.55, 128.29, 125.50, 109.23, 62.85, 32.31, 29.20, 26.06

4,4'-(5,5'-dibromo-[2,2'-bithiophene]-4,4'-diyl)bis(butan-1-ol) (7): General procedure 4 was applied to compound (6). Recrystallized twice in chloroform. Yield = 49%

^{1}H NMR ($CDCl_3$, 400MHz) δ: 6.78 (s, 2H), 3.68 (t, 4H, J=5.9Hz), 2.57 (t, 4H, J=7.2Hz), 1.72-1.56 (m, 8H), 1.31 (bs, 2H)

^{13}C NMR ($CDCl_3$, 400MHz) δ: 142.58, 136.41, 124.57, 108.38, 62.80, 32.29, 25.99

5,5'-dibromo-4,4'-bis(4-(heptyloxy)butyl)-2,2'-bithiophene (8): General procedure 5 was applied to compound (7) with 1-bromoheptane. Yield = 83%

^{1}H NMR ($CDCl_3$, 400MHz) δ: 6.77 (s, 2H), 3.42 (t, 4H, J=6.2Hz), 3.39 (t, 4H, J=6.2Hz), 2.55 (t, 4H, J=7.2Hz), 1.70-1.51 (m, 12H), 1.36-1.20 (m, 16H), 0.88 (t, 6H, J=7.05Hz)

^{13}C NMR ($CDCl_3$, 400MHz) δ: 142.69, 136.31, 124.53, 108.18, 71.19, 70.55, 31.95, 29.90, 29.42, 29.39, 29.30, 26.42, 26.30, 22.75, 14.22

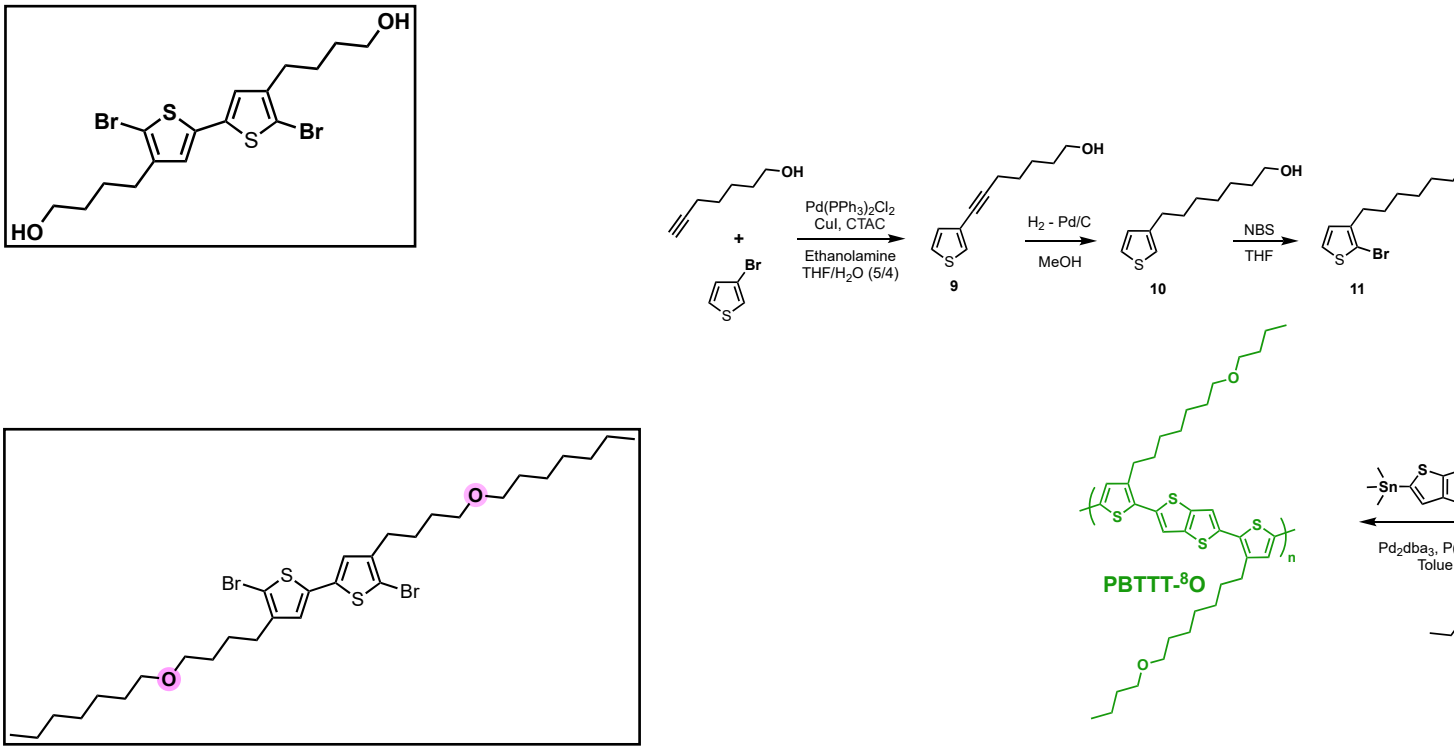

Scheme S4. Synthetic route towards the PBTTT-^{8}O.

7-(thiophen-3-yl)hept-6-yn-1-ol (9): General procedure 1 was applied to heptyn-1-ol with 3-bromothiophene. Yield 90%

^{1}H NMR ($CDCl_3$, 400MHz) δ: 7.34 (dd, 1H, J_1=3Hz, J_2=1.2Hz), 7.23 (dd, 1H, J_1=5Hz, J_2=3Hz), 7.06 (dd, 1H, J_1=5Hz, J_2=1.2Hz), 3.67 (t, 2H, J=6.4Hz), 2.41 (t, 2H, J=7Hz), 1.68-1.58 (m, 4H), 1.48-1.54 (m, 2H), 1.24 (bs, 1H)

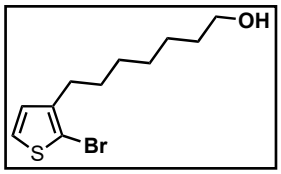

^{13}C NMR ($CDCl_3$, 400MHz) δ: 130.13, 127.71, 125.14, 123.04, 89.68, 75.90, 63.03, 32.44, 28.63, 25.24, 19.51

7-(thiophen-3-yl)heptan-1-ol (10): General procedure 2 was applied to compound (9). Yield 80%

^{1}H NMR ($CDCl_3$, 400MHz) δ: 7.23 (dd, 1H, J_1=4.9HZ, J_2=2.9Hz), 6.92 (m,2H), 3.60 (td, 2H, J_1=6.7Hz), 2.62 (t, 2H, J=7.8Hz), 1.67-1.51 (m, 4H), 1.39-1.29 (m, 6H), 1.24 (bs, 1H)

^{13}C NMR ($CDCl_3$, 400MHz) δ: 143.27, 128.40, 125.21, 119.94, 63.18, 32.90, 30.61, 30.38, 29.39, 29.37, 25.81

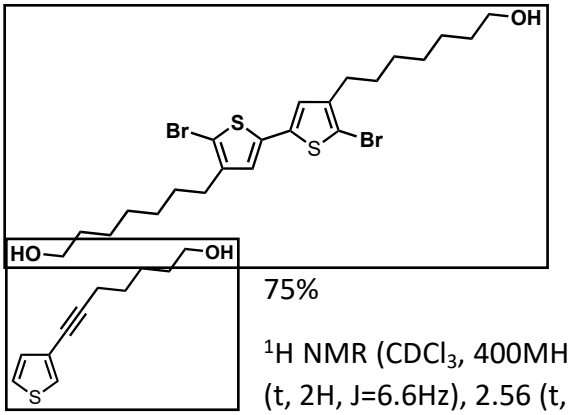

7-(2-bromothiophen-3-yl)heptan-1-ol (11): General procedure 3 was applied to compound (10). Yield 75%

^{1}H NMR ($CDCl_3$, 400MHz) δ: 7.18 (d, 1H, J=5.6Hz), 6.79 (d, 1H, J=5.6Hz), 3.64 (t, 2H, J=6.6Hz), 2.56 (t, 2H, J=7.6Hz), 1.62-1.52 (m, 4H), 1.38-1.32 (m, 6H)

^{13}C NMR ($CDCl_3$, 400MHz) δ: 142.00, 128.36, 125.33, 108.99, 63.18, 32.89, 29.78, 29.48, 29.31, 29.26, 25.79

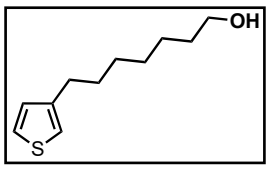

7,7'-(5,5'-dibromo-[2,2'-bithiophene]-4,4'-diyl)bis(heptan-1-ol) (12): General procedure 4 was applied to compound (11). Recrystallized twice in DCM. Yield 50%

^{1}H NMR ($CDCl_3$, 400MHz) δ: 6.77 (s, 2H), 3.64 (t, 4H, J=6.6Hz), 2.52 (t, 4H, J=7.7Hz), 1.64-1.52 (m, 8H), 1.4-1.32 (m, 12H)

^{13}C NMR ($CDCl_3$, 400MHz) δ: 143.00, 136.32, 124.60, 108.09, 63.18, 32.89, 29.68, 29.65, 29.30, 29.25, 25.79

5,5'-dibromo-4,4'-bis(7-butoxyheptyl)-2,2'-bithiophene (13): General procedure 5 was applied to compound (12) and 1-bromobutane. Yield = 75 %.

^{1}H NMR ($CDCl_3$, 400MHz) δ: 6.76(s, 2H), 3.40 (t, 4H, J=6.7Hz), 3.39 (t, 4H, J=6.7Hz), 2.51 (t, 4H, J=7.71Hz) 1.65-1.50 (m, 12H), 1.42-1.30 (m, 16H), 0.92 (t, 6H, J=7.4Hz)

^{13}C NMR ($CDCl_3$, 400MHz) δ: 143.03, 136.31, 124.58, 108.03, 71.03, 70.80, 32.02, 29.89, 29.7, 29.66, 29.37, 29.26, 26.25, 19.52, 14.09

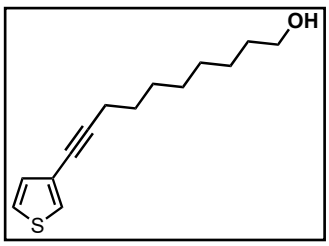

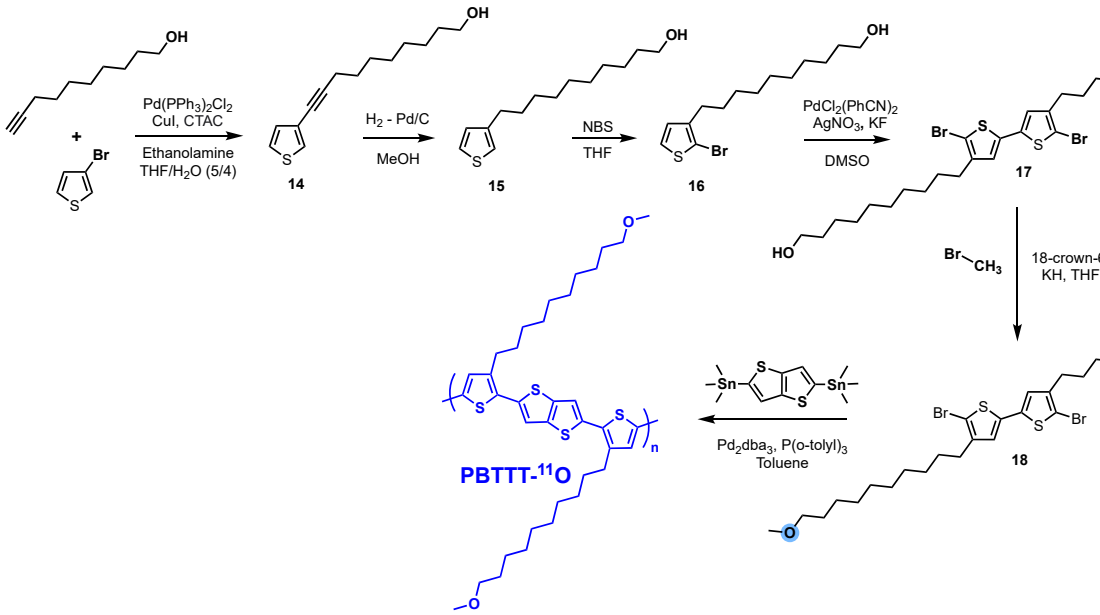

Scheme S5. Synthetic route towards the PBTTT-^{11}O.

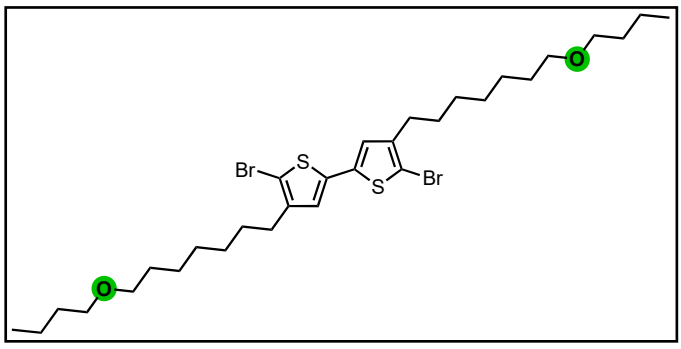

10-(thiophen-3-yl)dec-9-yn-1-ol (14): General procedure 1 was applied to decyn-1-ol with 3-bromothiophene. Yield = 74%

^{1}H NMR ($CDCl_3$, 400MHz) δ: 7.32 (dd, 1H, J_1=3.1Hz, J_2=1.2Hz), 7.2 (dd, 1H, J_1=5.0Hz,

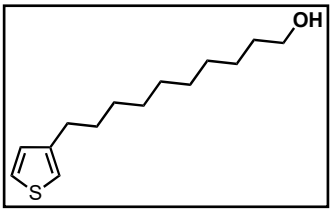

J_2=2.0Hz), 7.05 (dd, 1H, J_1=5.0Hz, J_2=1.2Hz), 3.59 (t, 2H, J=6.7Hz), 2.36 (t, 2H, J=7.1Hz), 1.97 (bs, 1H) 1.62-1.49 (m, 4H), 1.48-1.36 (m, 2H), 1.36-1.25 (m, 6H)

^{13}C NMR ($CDCl_3$, 400MHz) δ: 129.97, 127.47, 122.97, 89.87, 75.65, 62.76, 32.69, 29.30, 29.10, 28.85, 28.69, 25.72, 19.36

10-(thiophen-3-yl)decan-1-ol (15): General procedure 2 was applied to compound (14). Yield = 93%

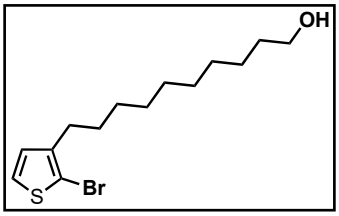

^{1}H NMR ($CDCl_3$, 400MHz) δ: 7.23 (dd, 1H, J_1=4.9Hz, J_2=2.9Hz), 6.92 (m, 2H), 3.63 (t, 2H, J=6.7Hz), 2.62 (t, 2H, J=7.3Hz), 1.66-1.50 (m, 2H), 1.39-1.23 (m, 14H)

^{13}C NMR ($CDCl_3$, 400MHz) δ: 143.35, 128.40, 125.14, 119.87, 63.16, 32.90, 30.67, 30.39, 29.70, 29.62, 29.56, 29.53, 29.43, 25.85

10-(2-bromothiophen-3-yl)decan-1-ol (16): General procedure 3 was applied to compound (15). Yield = 69%

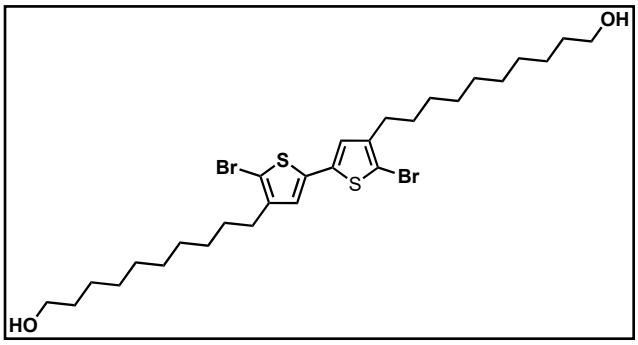

^{1}H NMR ($CDCl_3$, 400MHz) δ: 7.16 (d, 1H, J=5.6Hz), 6.78 (d, 1H, J=5.6Hz), 3.61 (t, 2H, J=6.7Hz), 2.55 (t, 2H, J=7.6Hz), 1.94 (s, 1H), 1.60-1.54 (m, 2H), 1.27-1.35 (m, 14H)

^{13}C NMR ($CDCl_3$, 400MHz) δ: 141.99, 128.28, 125.20, 108.83, 62.99, 32.82, 29.78, 29.64, 29.55, 29.49, 29.43, 29.25, 25.81

10,10'-(5,5'-dibromo-[2,2'-bithiophene]-4,4'-diyl)bis(decan-1-ol) (17): General procedure 4 was applied to compound (16). Recrystallized twice in DCM. Yield = 55%.

^{1}H NMR ($CDCl_3$, 400MHz) δ: 6.77 (s, 2H), 3.64 (t, 4H, J=6.6Hz), 2.51 (t, 4H, J=7.6Hz), 1.61-1.51 (m, 4H), 1.48 (bs, 2H), 1.35-1.25 (m, 28H)

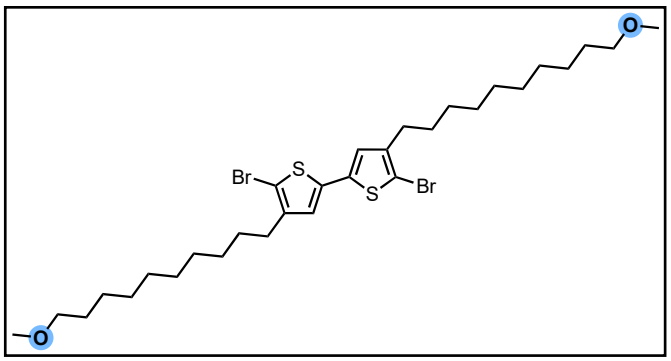

^{13}C NMR ($CDCl_3$, 400MHz) δ: 143.08, 136.29, 124.59, 108.01, 63.21, 32.94, 29.74, 29.70, 29.67, 29.59, 29.54, 29.49, 29.29, 25.86

5,5'-dibromo-4,4'-bis(10-methoxydecyl)-2,2'-bithiophene (18): General procedure 5 was applied to compound (17) with methyl iodide. Yield = 81%

^{1}H NMR ($CDCl_3$, 400MHz) δ: 6.77 (s, 2H), 3.36 (t, 4H, J=6.7Hz), 3.33 (s, 6H), 2.52 (t, 4H, J=7.7Hz), 1.59-1.53 (m, 4H), 1.33-1.27 (m, 28H)

^{13}C NMR ($CDCl_3$, 400MHz) δ: 143.11, 136.31, 124.61, 108.01, 73.12, 58.69, 29.81, 29.76, 29.70, 29.63, 29.61, 29.50, 29.33, 26.28

PS: *It is worth noting that when the ether function is present at either ends of the side chains (i.e. BT-^{3}O or BT-^{11}O), the bithiophenes are solid and crystalline at room temperature. However, when the ether function is in the middle of the side chains (i.e. BT-^{5}O or BT-^{8}O), the bithiophenes remain liquid at room temperature.*

NMR traces

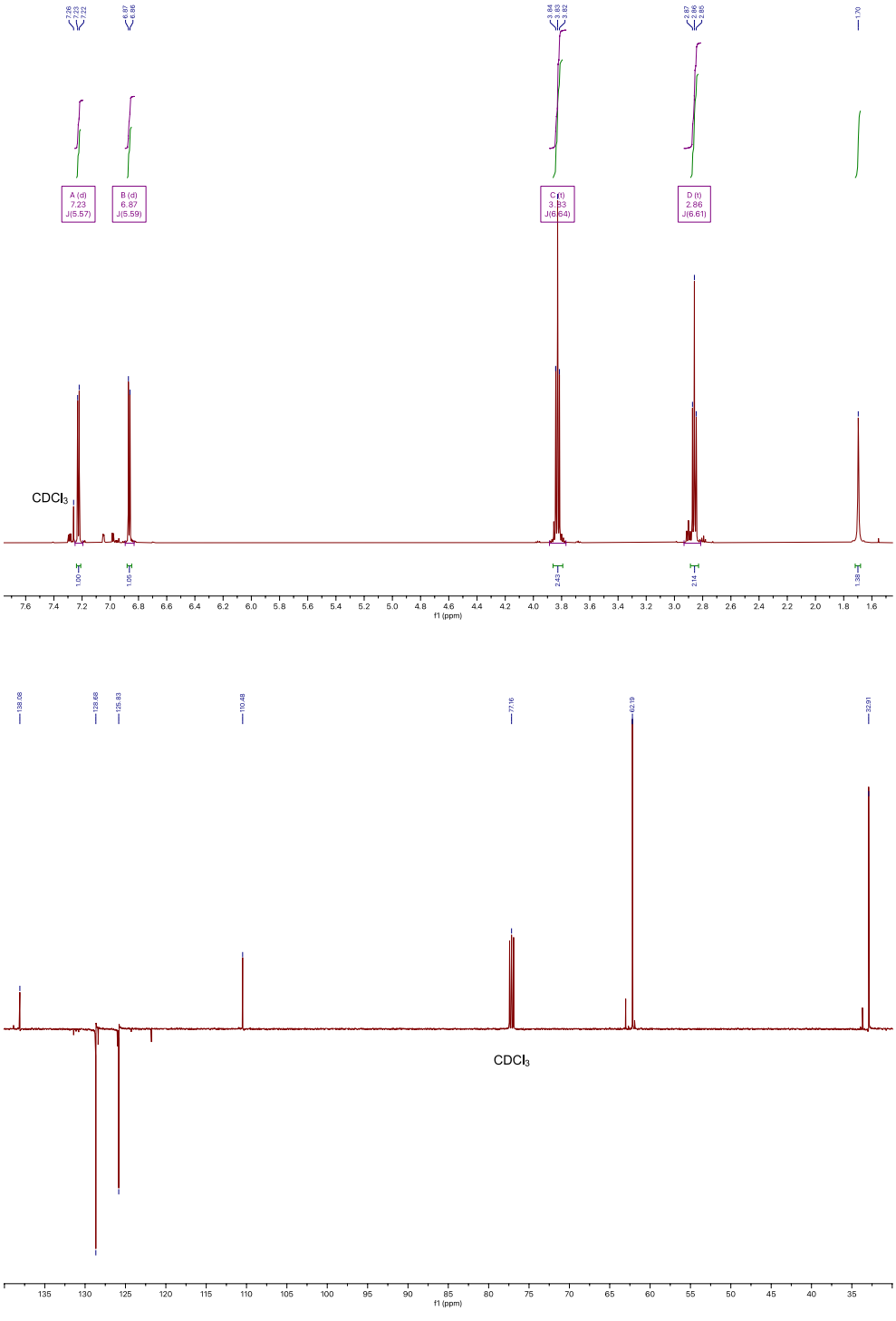

Figure S1. (top) ^{1}H and (bottom) ^{13}C NMR traces of compound **1** in $CDCl_3$.

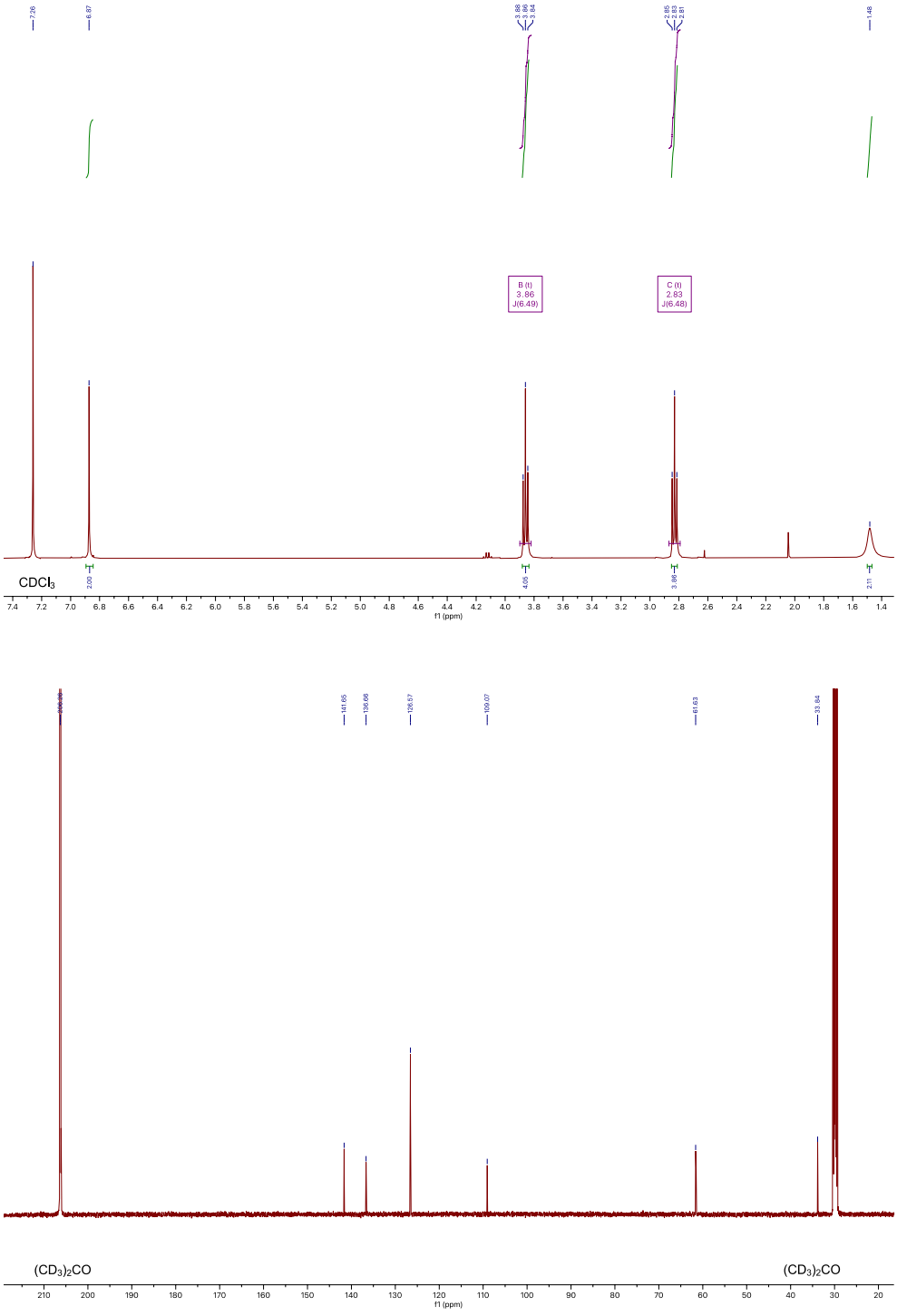

Figure S2. (top) ^{1}H and (bottom) ^{13}C NMR traces of compound **2** in $CDCl_3$ and $(CD_3)_2CO$, respectively.

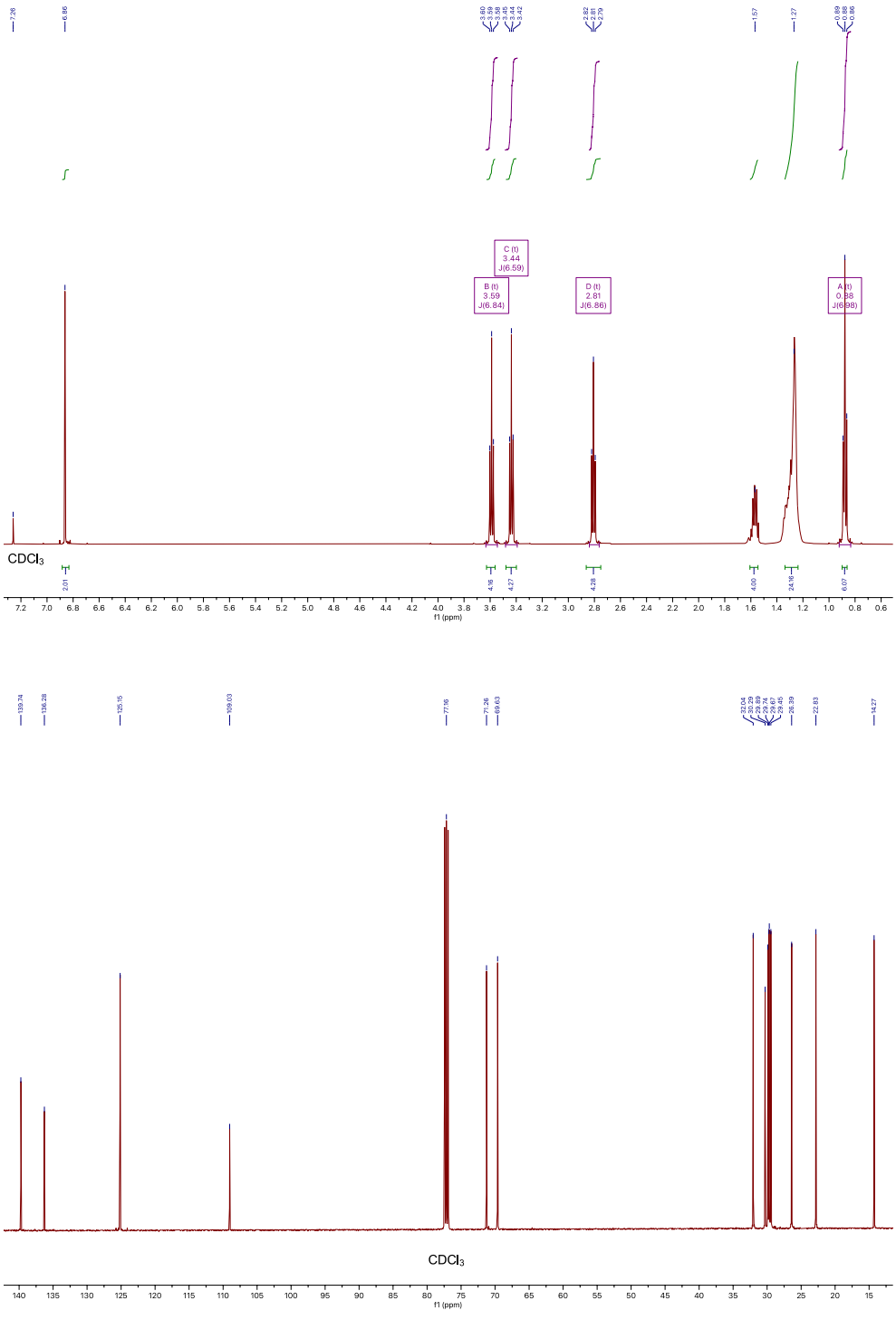

Figure S3. (top) ^{1}H and (bottom) ^{13}C NMR traces of compound **3** in $CDCl_3$.

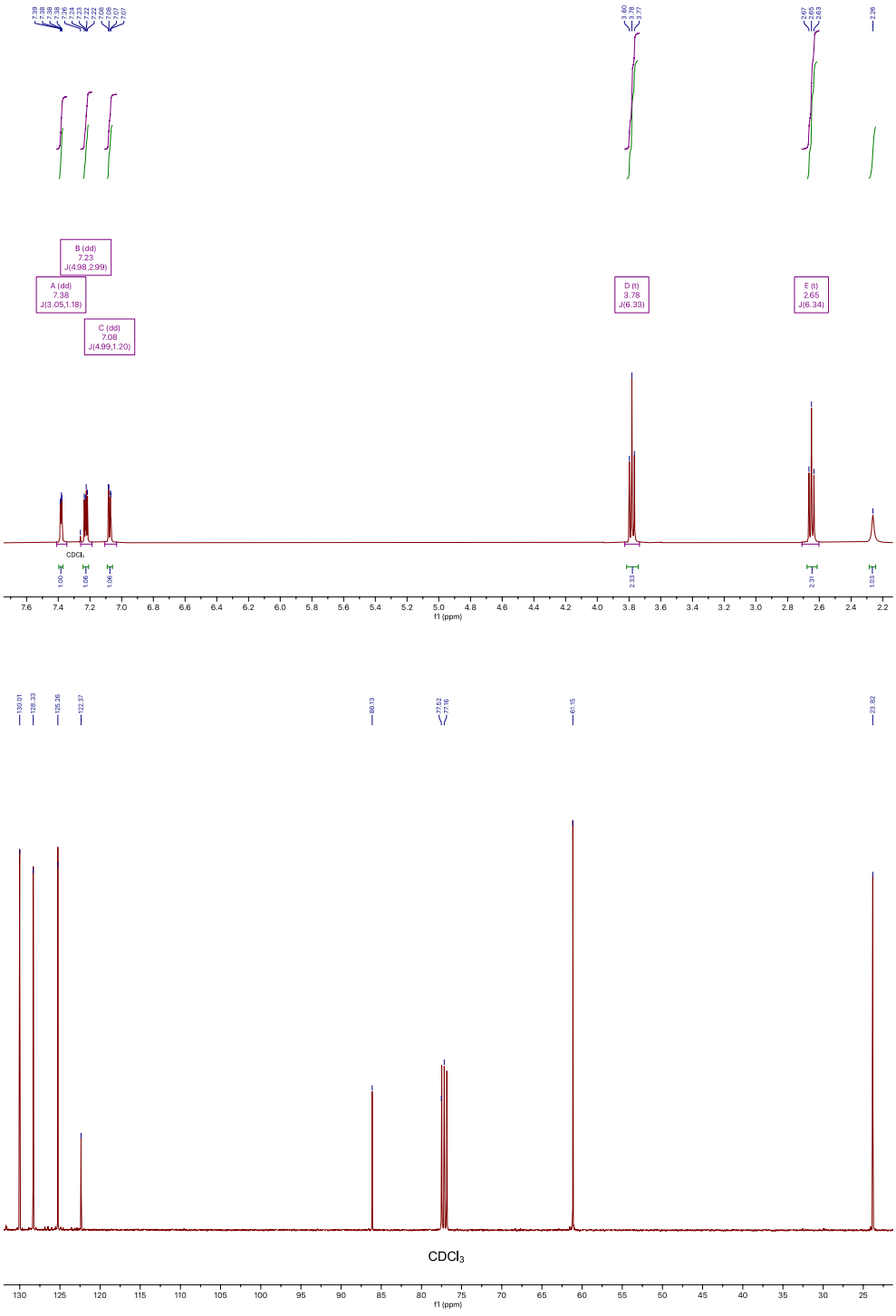

Figure S4. (top) ^{1}H and (bottom) ^{13}C NMR traces of compound **4** in $CDCl_3$.

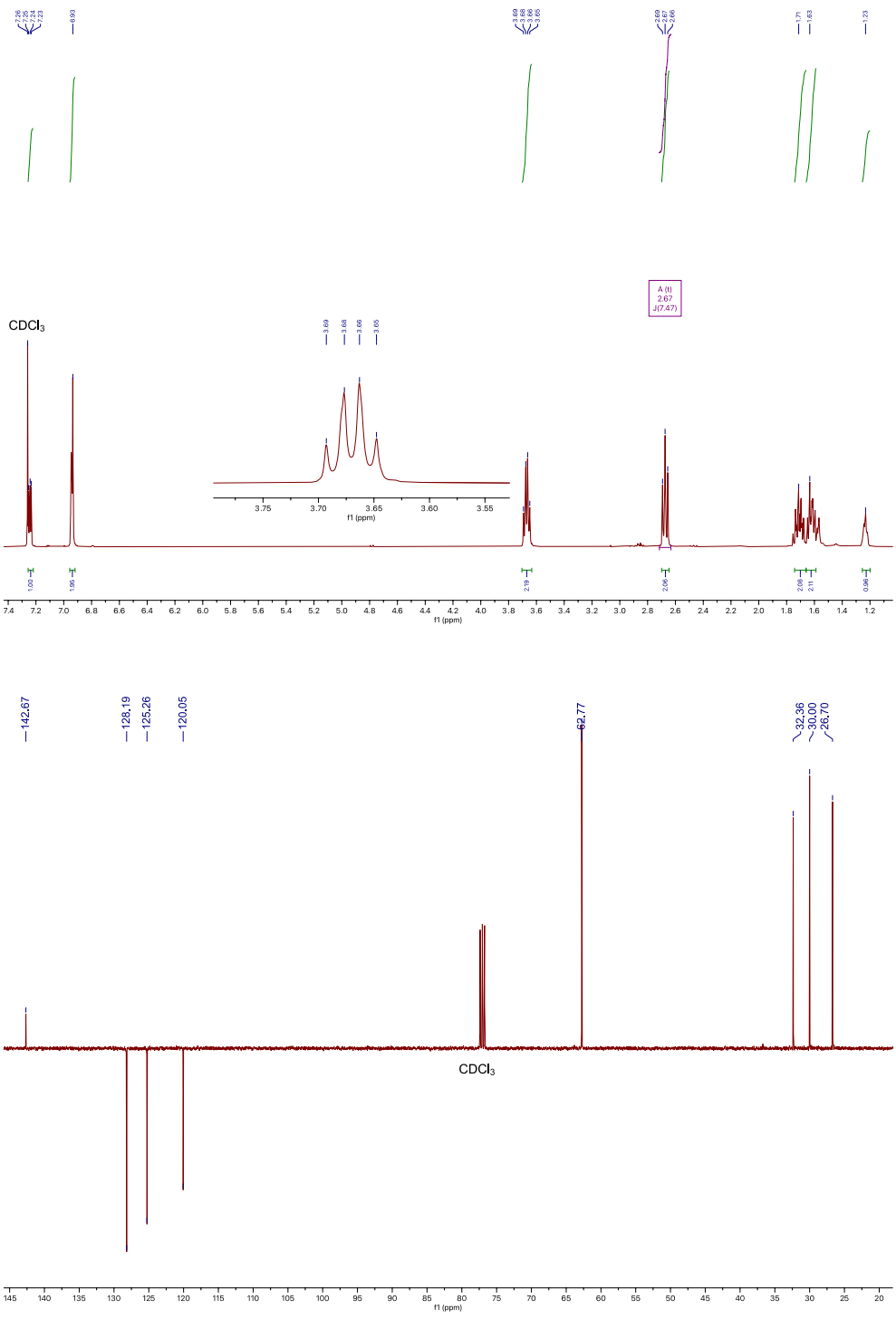

Figure S5. (top) ^{1}H and (bottom) ^{13}C NMR traces of compound **5** in $CDCl_3$.

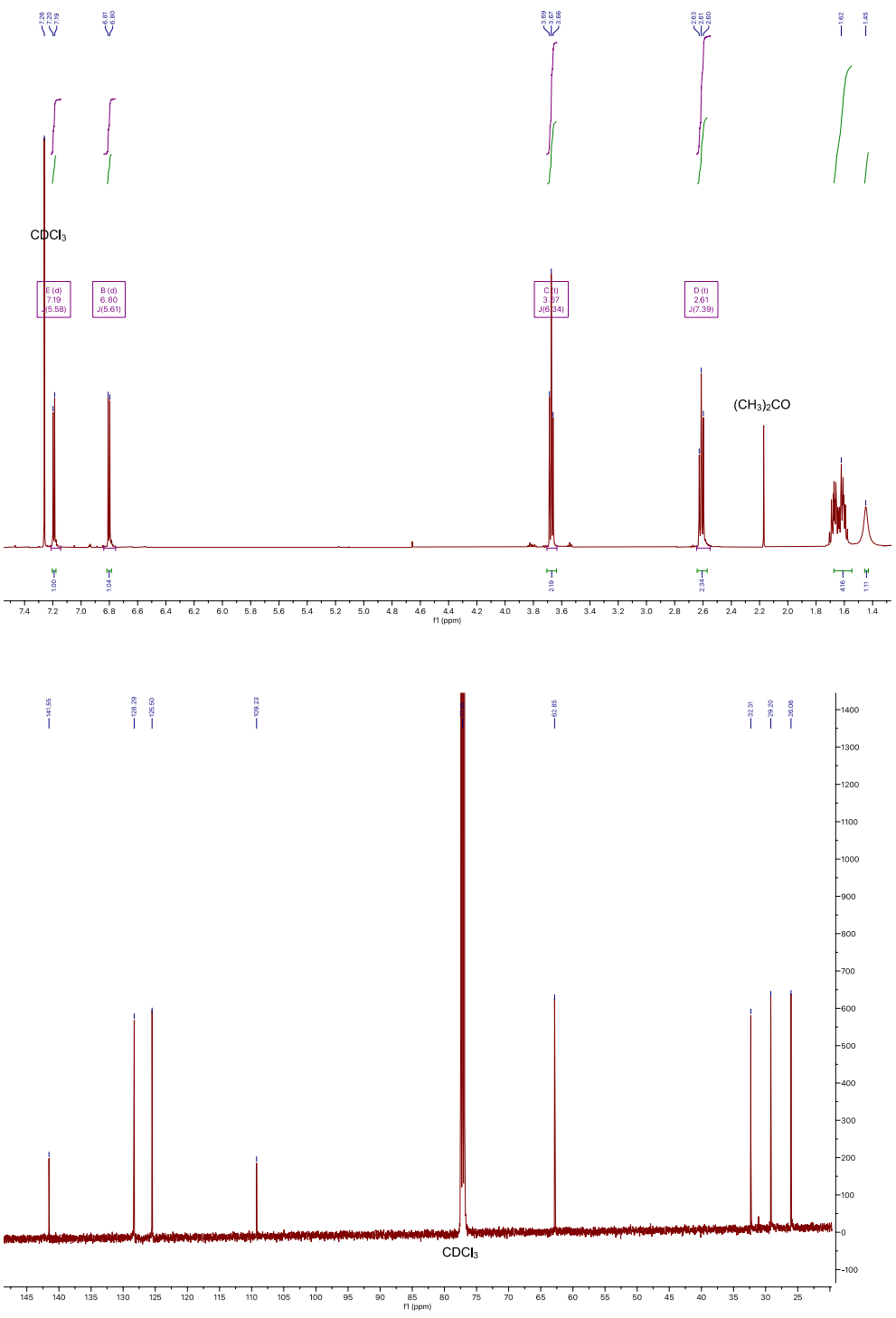

Figure S6. (top) ^{1}H and (bottom) ^{13}C NMR traces of compound **6** in $CDCl_3$.

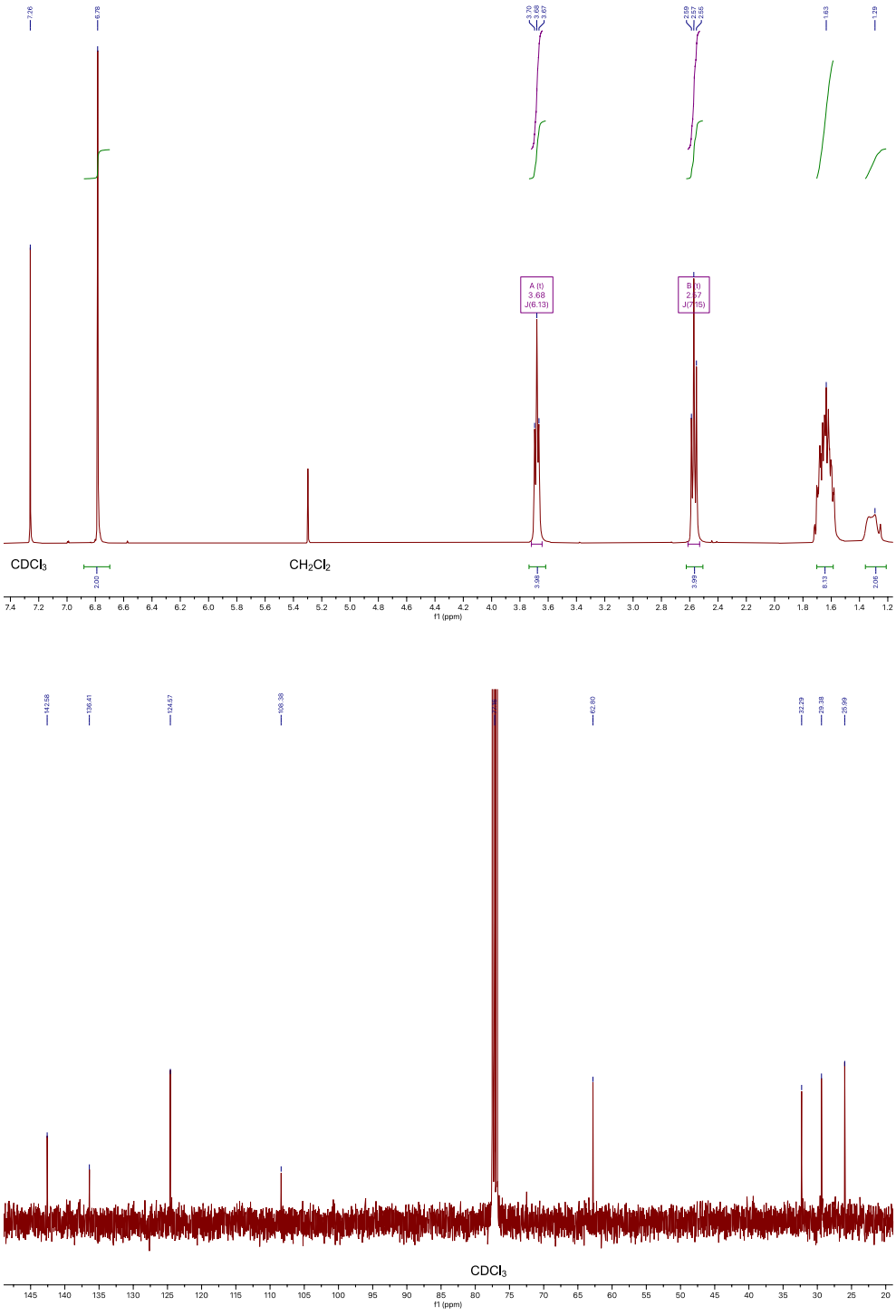

Figure S7. (top) ^{1}H and (bottom) ^{13}C NMR traces of compound **7** in $CDCl_3$.

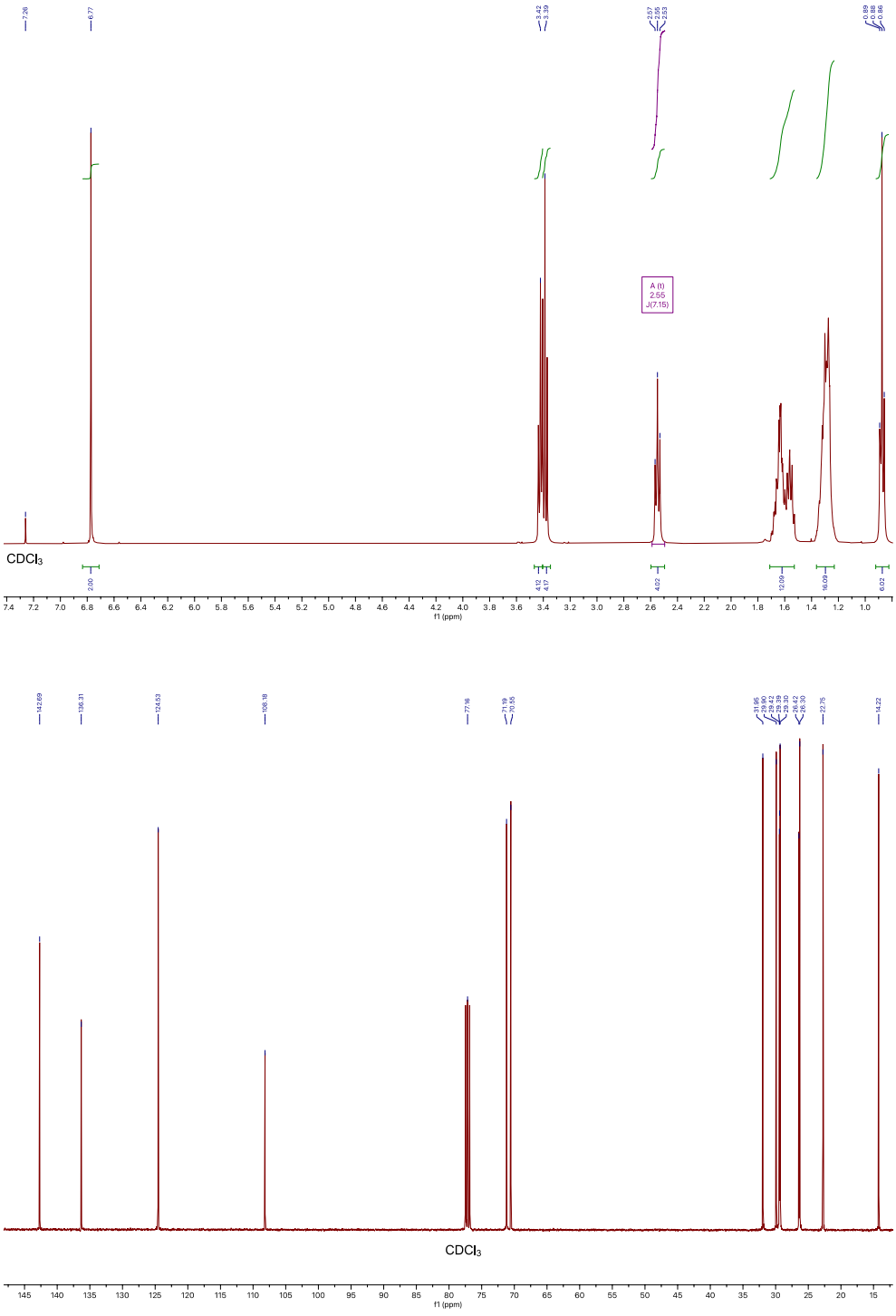

Figure S8. (top) ^{1}H and (bottom) ^{13}C NMR traces of compound **8** in $CDCl_3$.

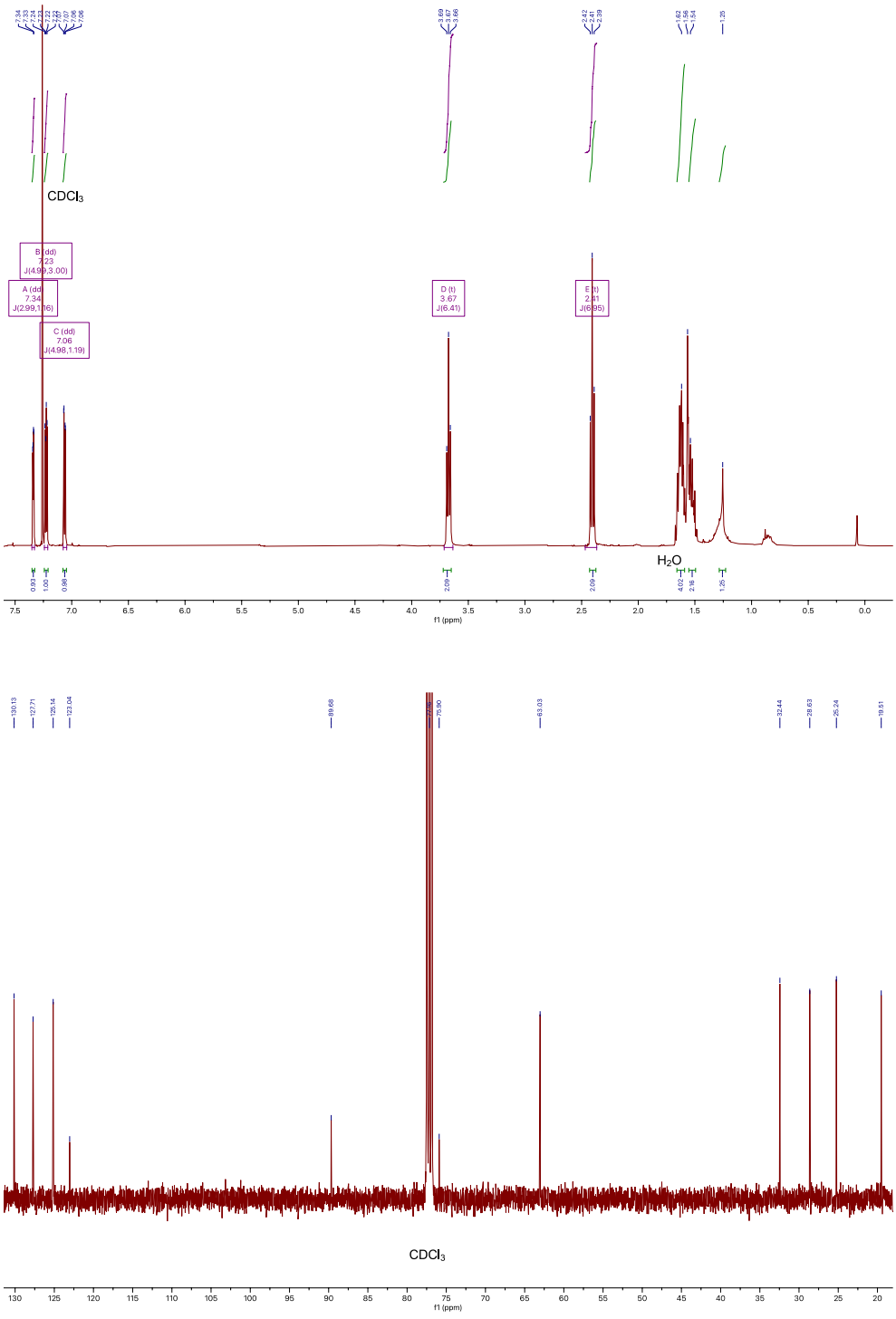

Figure S9. (top) ^{1}H and (bottom) ^{13}C NMR traces of compound **9** in $CDCl_3$.

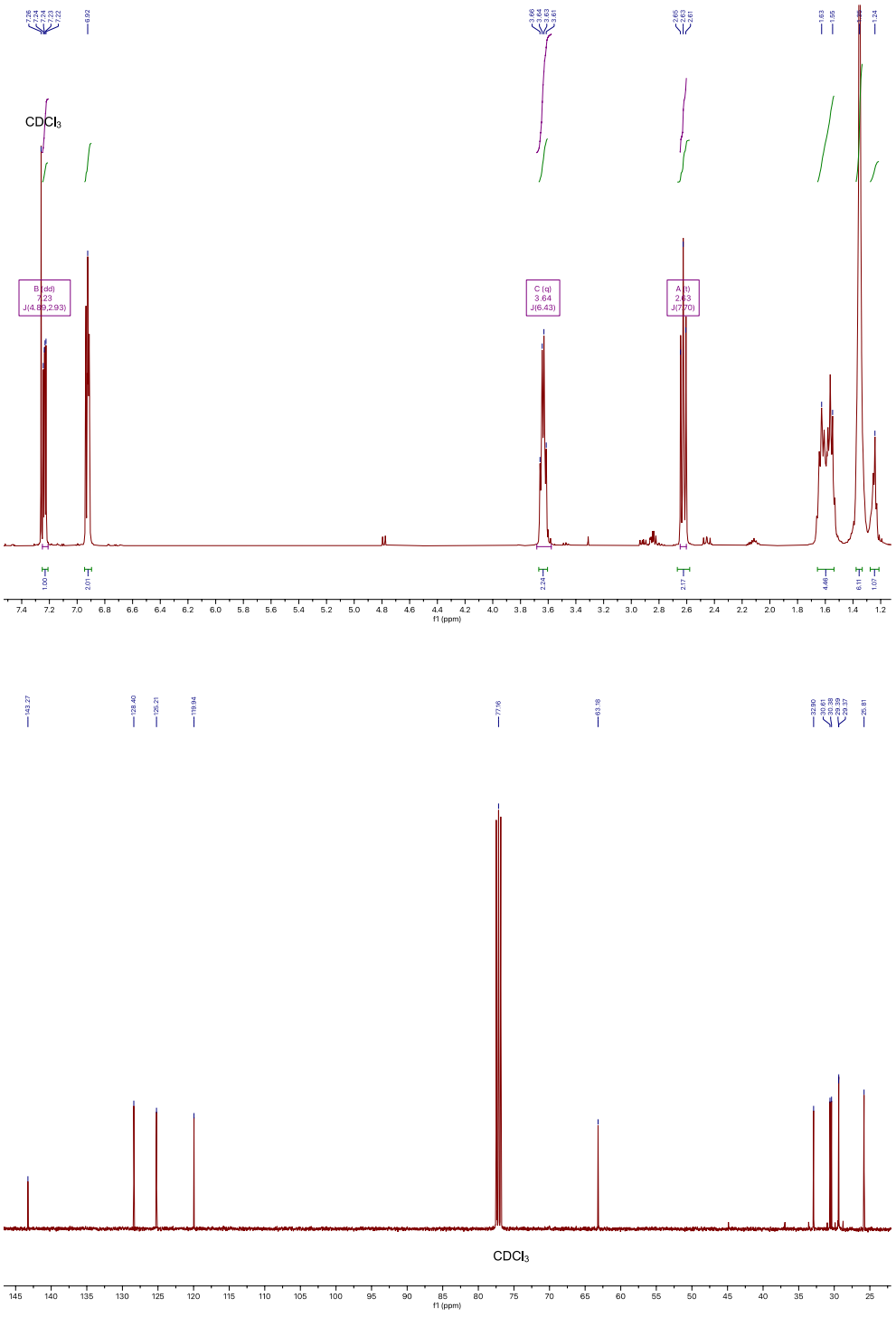

Figure S10. (top) ^{1}H and (bottom) ^{13}C NMR traces of compound **10** in $CDCl_3$.

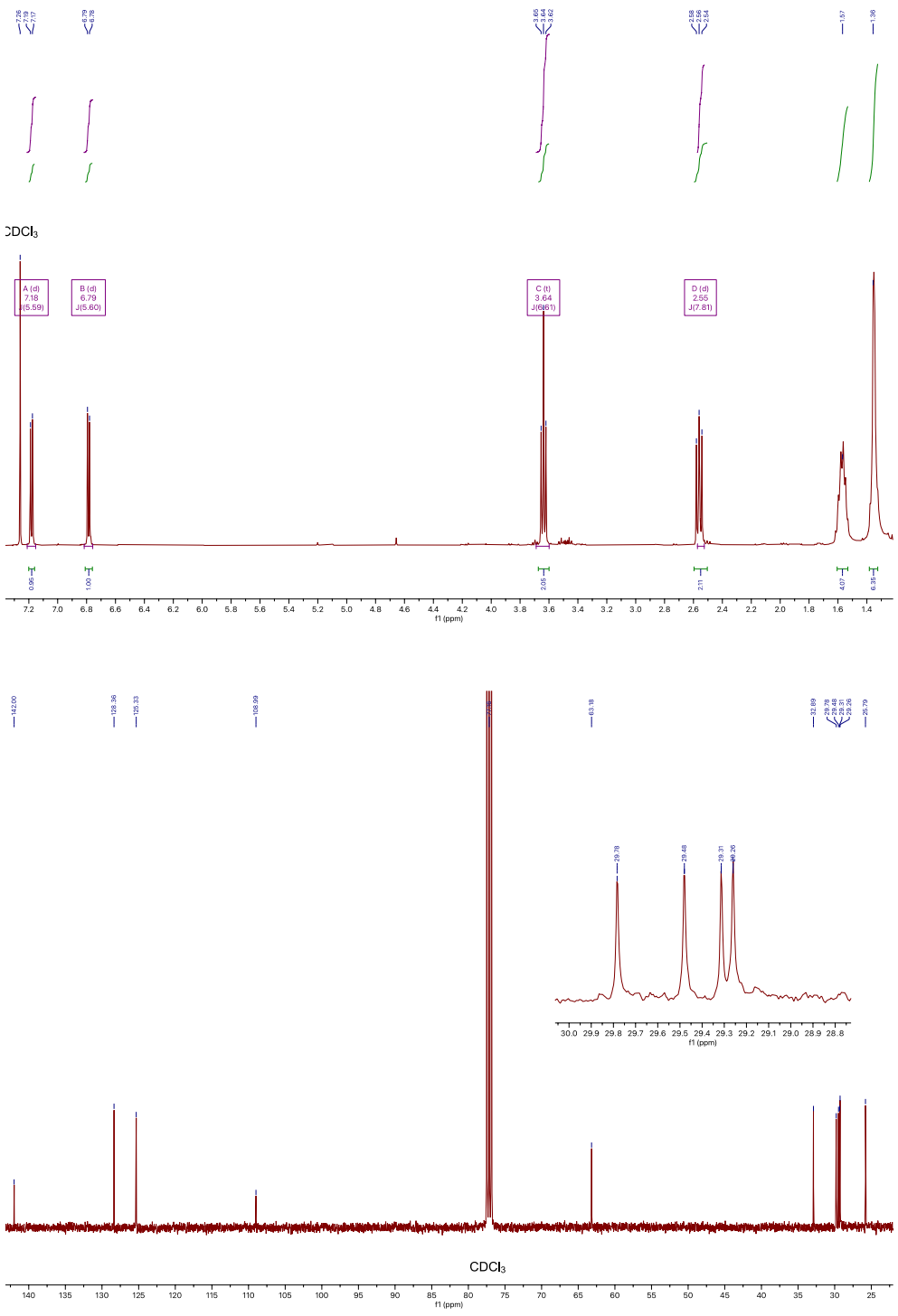

Figure S11. (top) ^{1}H and (bottom) ^{13}C NMR traces of compound **11** in $CDCl_3$.

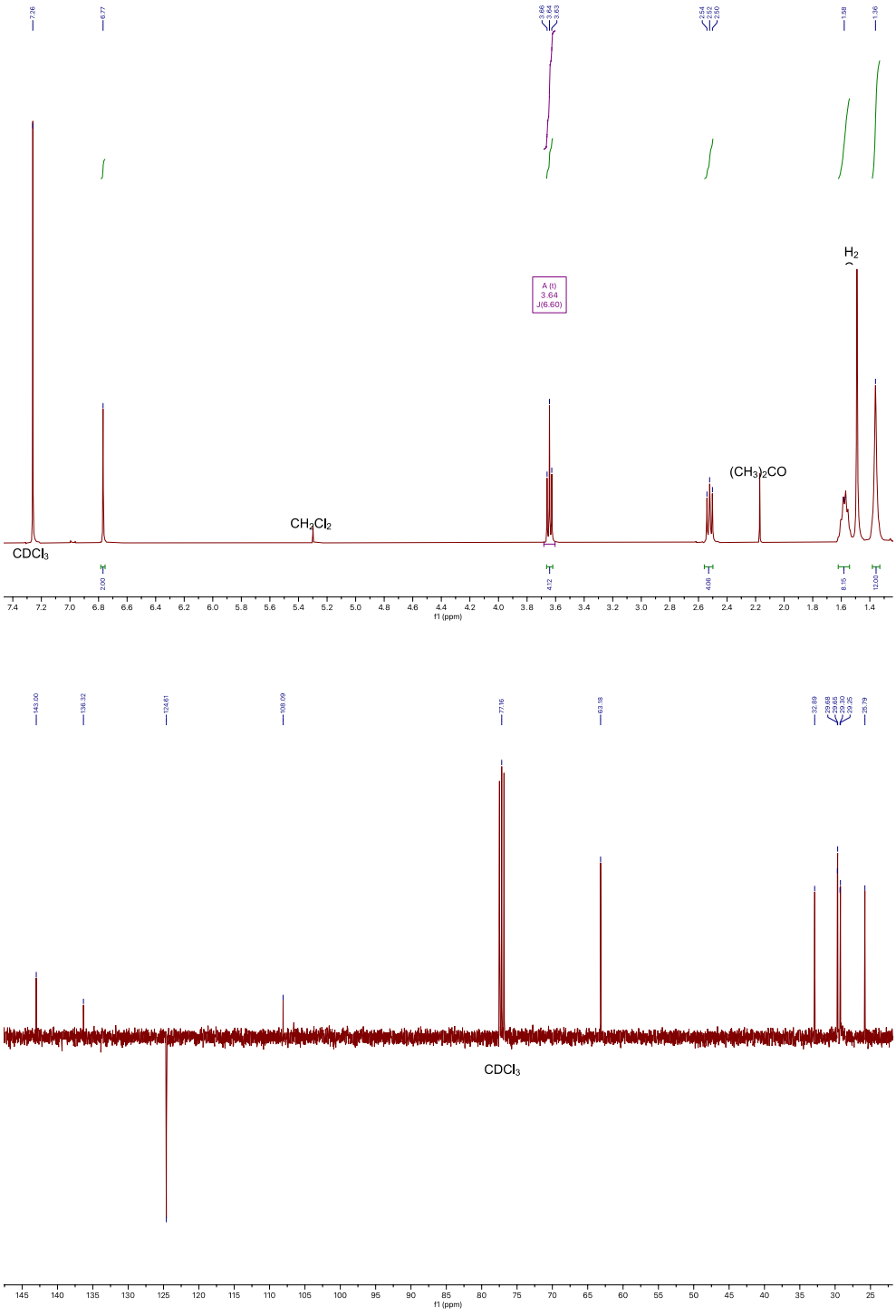

Figure S12. (top) ^{1}H and (bottom) ^{13}C NMR traces of compound **12** in $CDCl_3$.

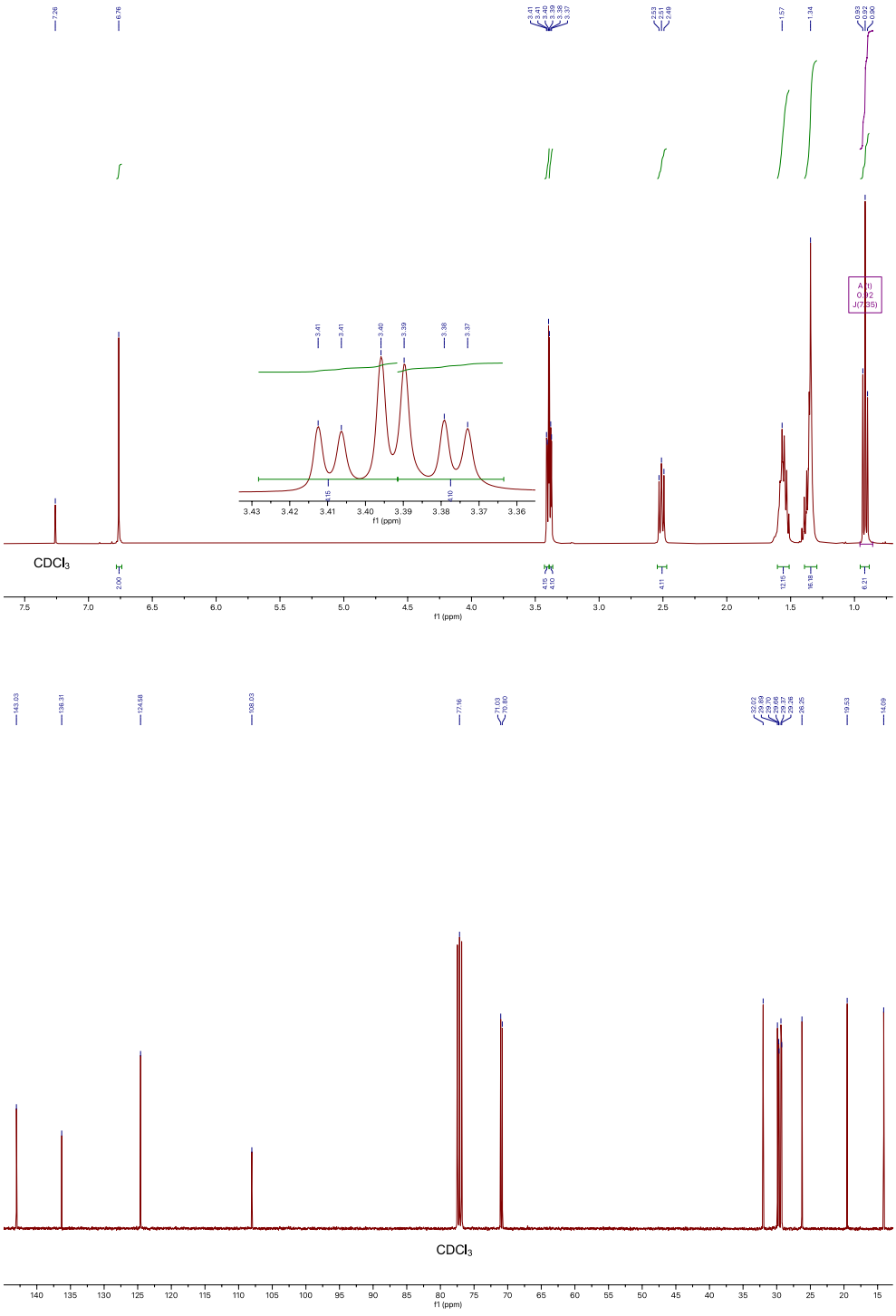

Figure S13. (top) ^{1}H and (bottom) ^{13}C NMR traces of compound **13** in $CDCl_3$.

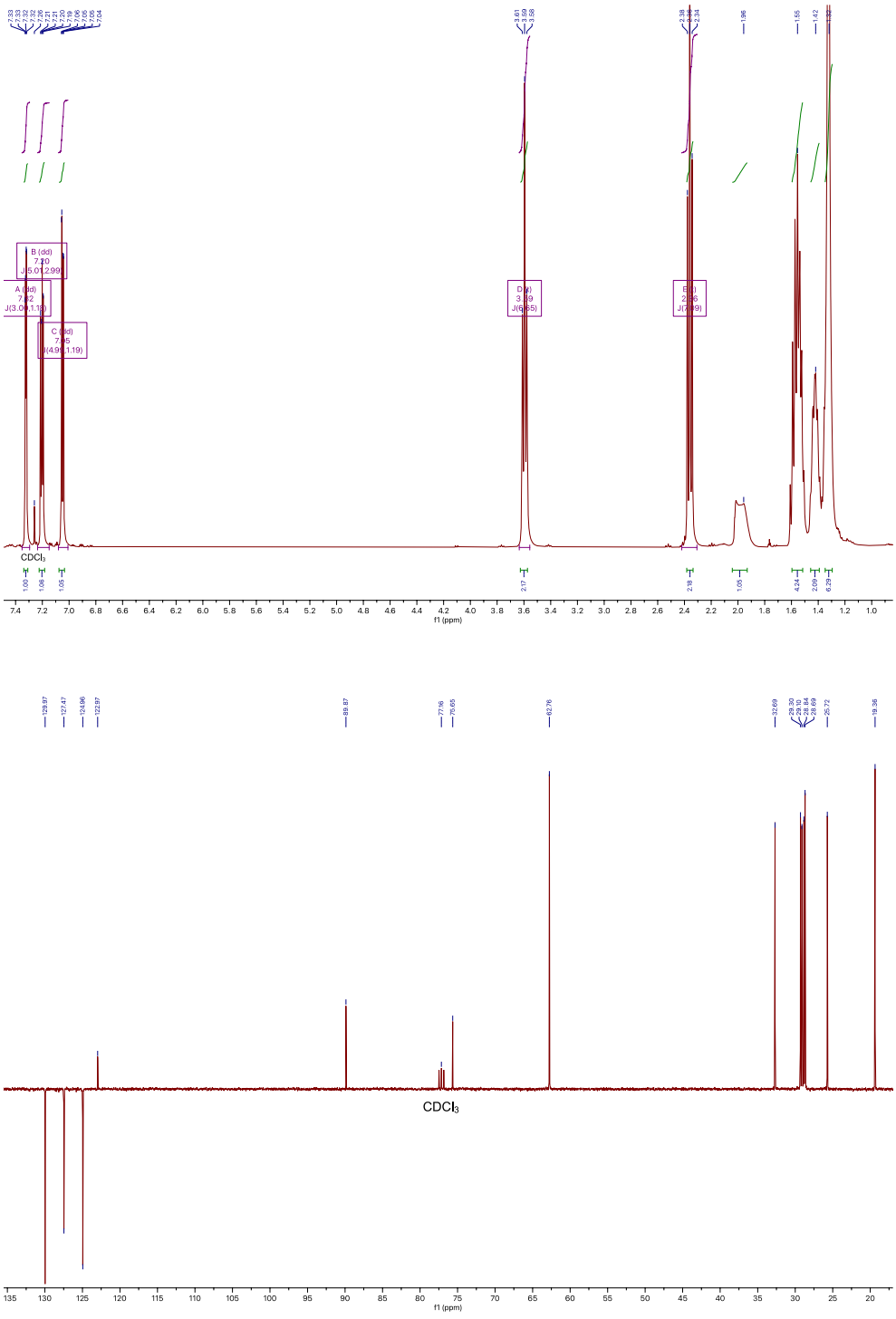

Figure S14. (top) ^{1}H and (bottom) ^{13}C NMR traces of compound **14** in $CDCl_3$.

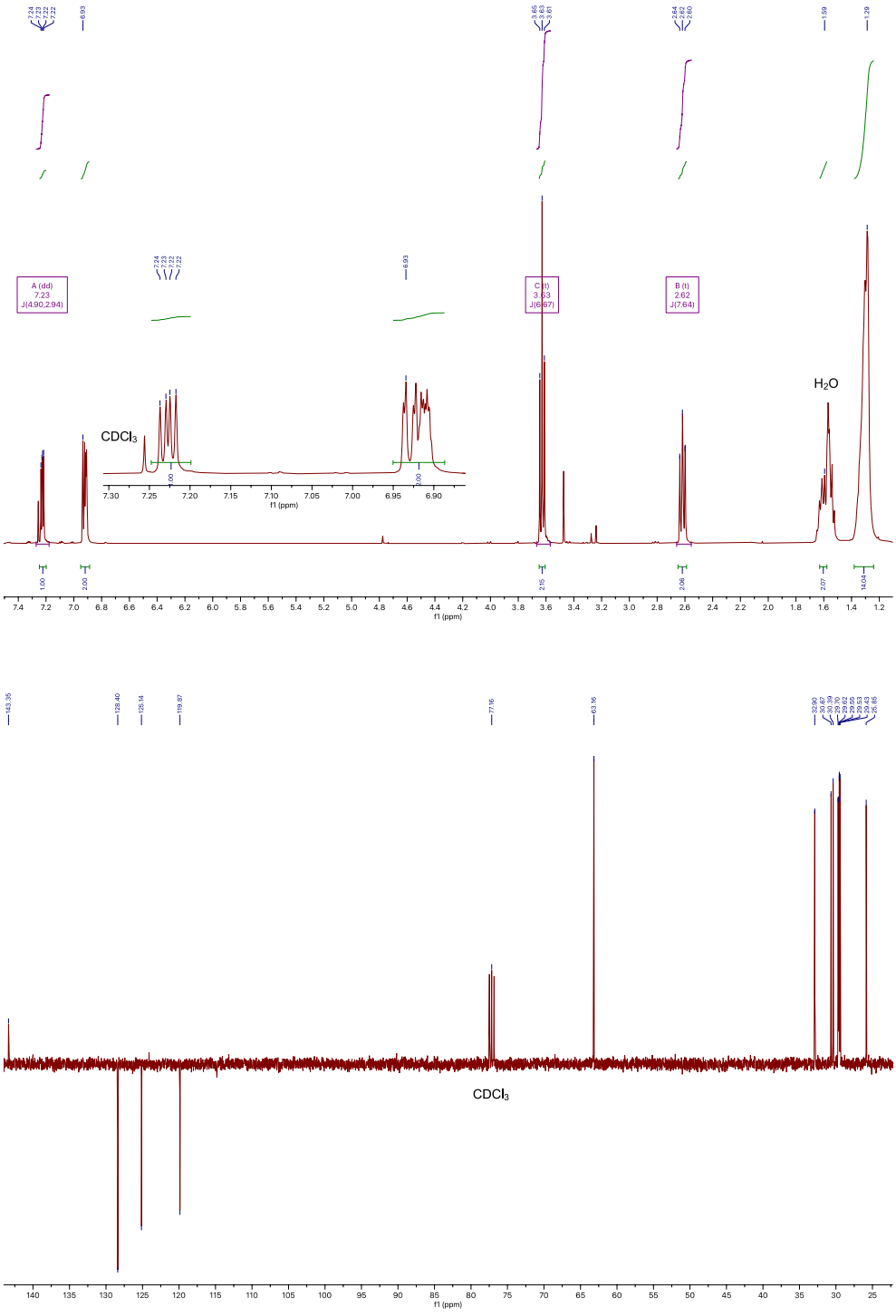

Figure S15. (top) ^{1}H and (bottom) ^{13}C NMR traces of compound **15** in $CDCl_3$.

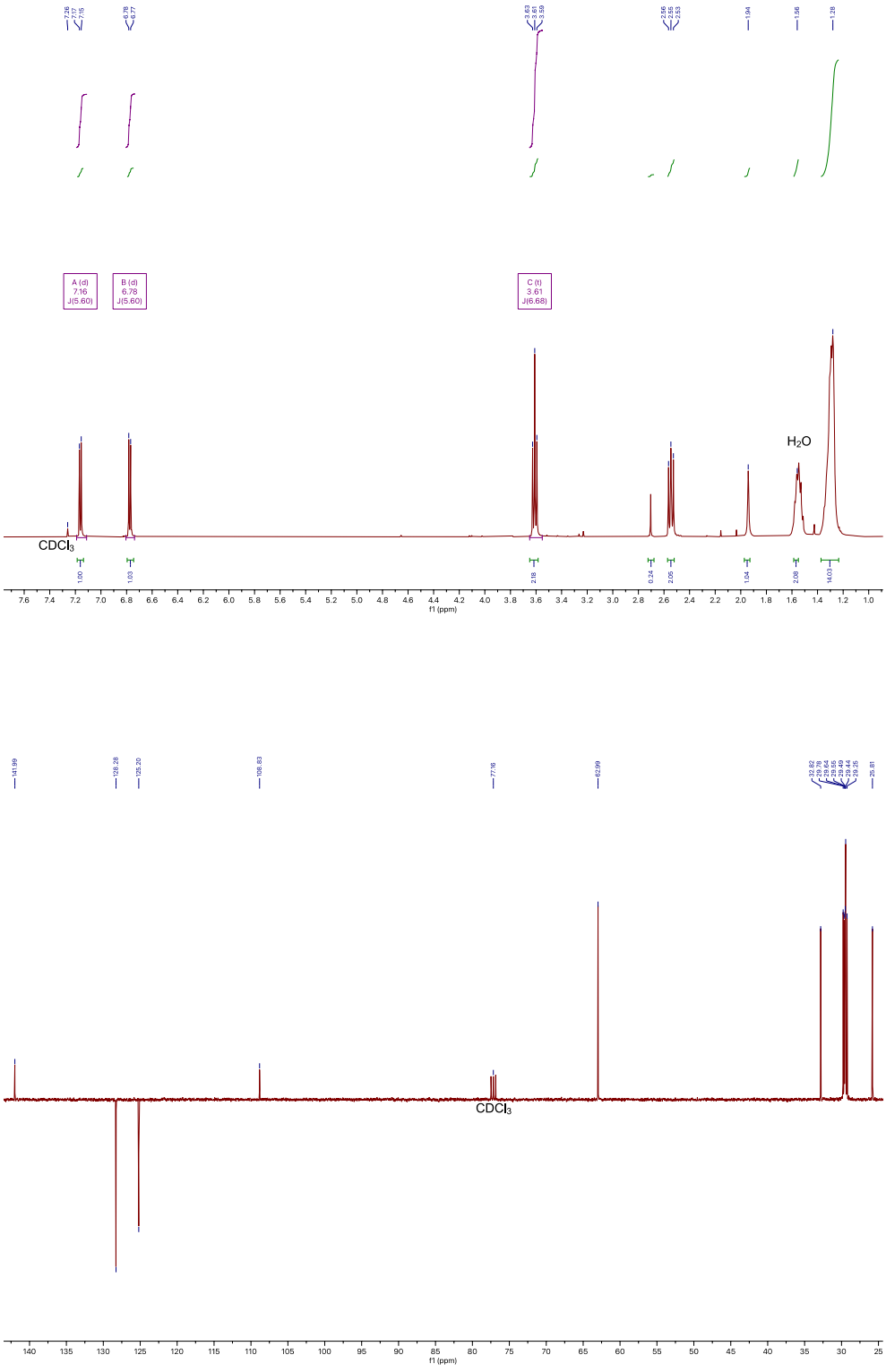

Figure S16. (top) ^{1}H and (bottom) ^{13}C NMR traces of compound **16** in $CDCl_3$.

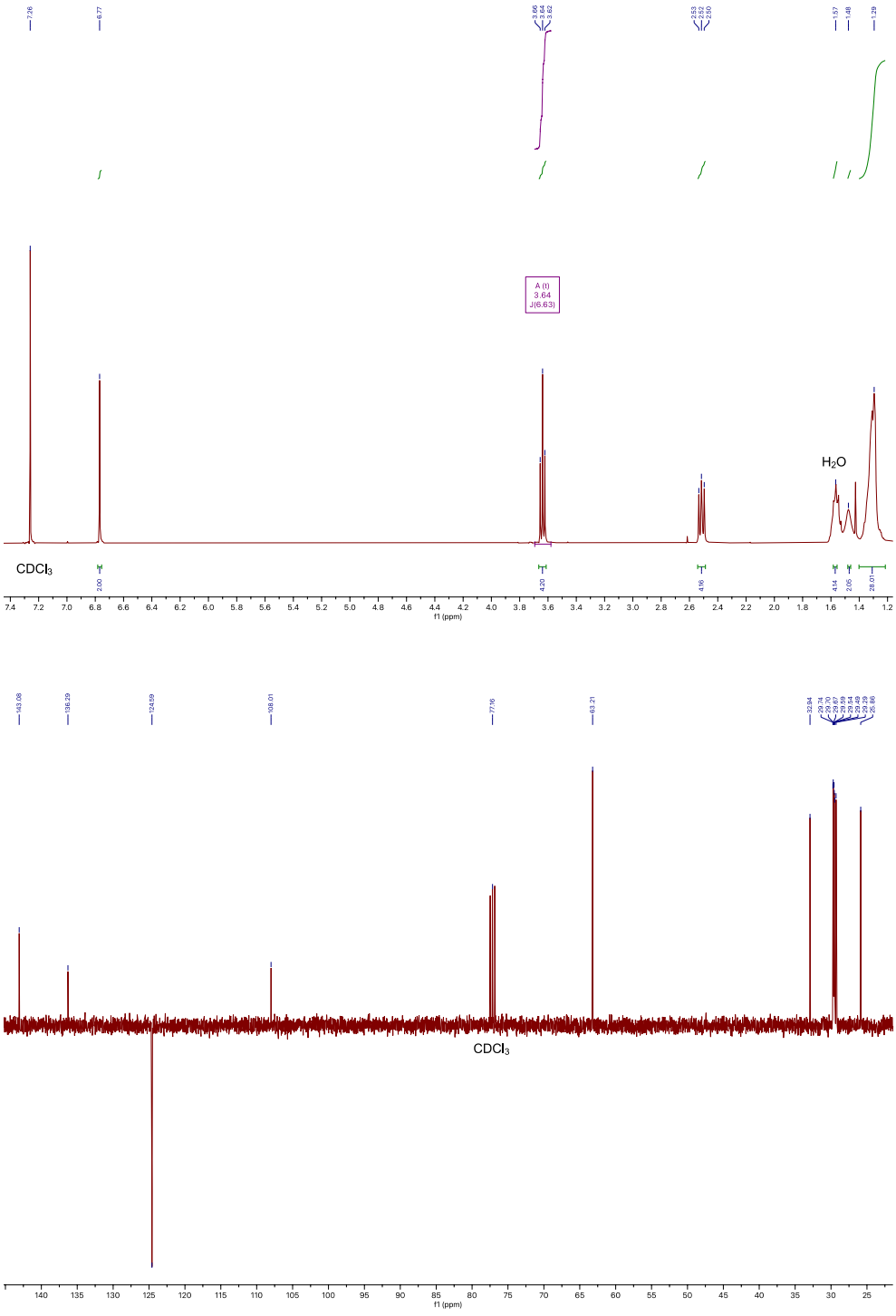

Figure S17. (top) ^{1}H and (bottom) ^{13}C NMR traces of compound **17** in $CDCl_3$.

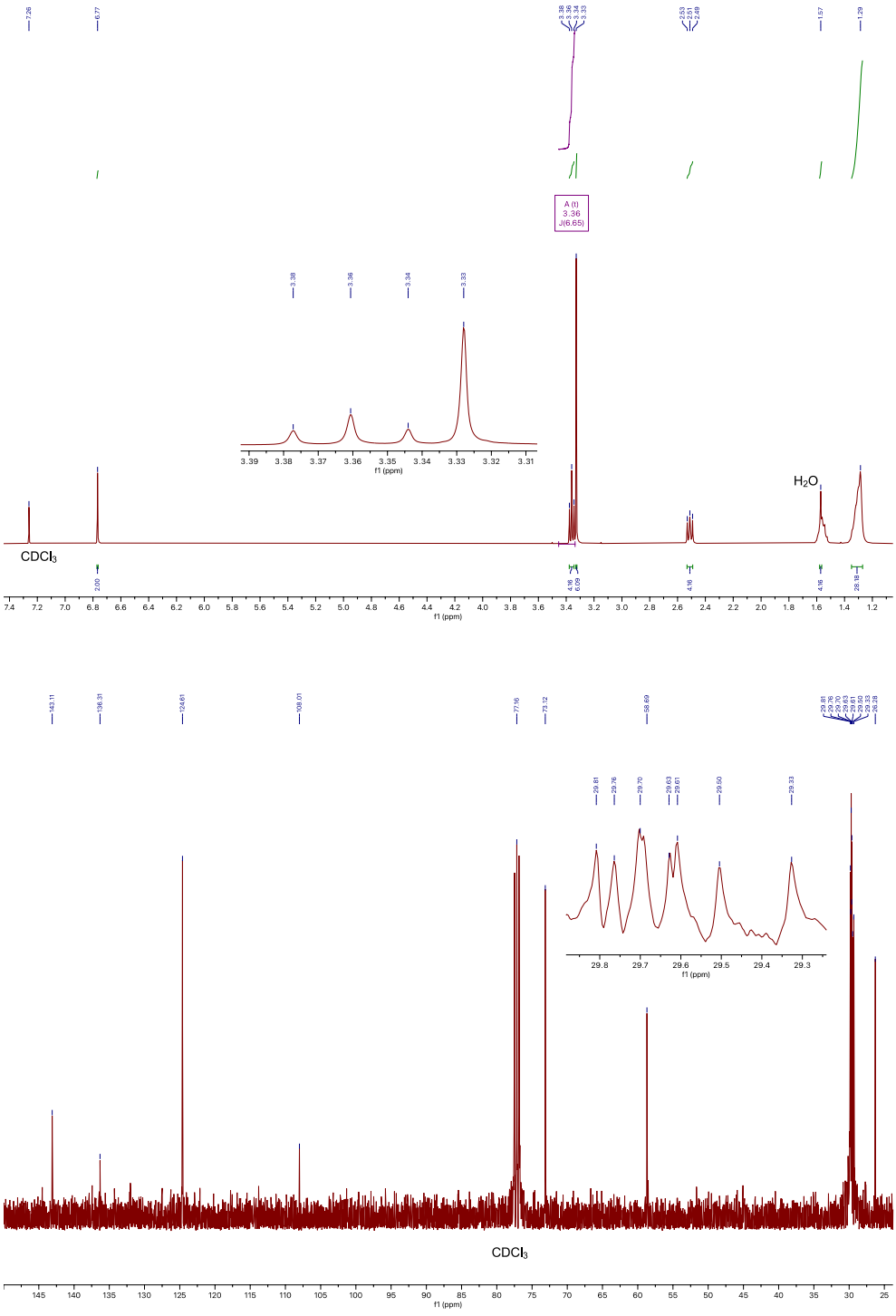

Figure S18. (top) ^{1}H and (bottom) ^{13}C NMR traces of compound **18** in $CDCl_3$.

SIze Exclusion Chromatography (SEC)

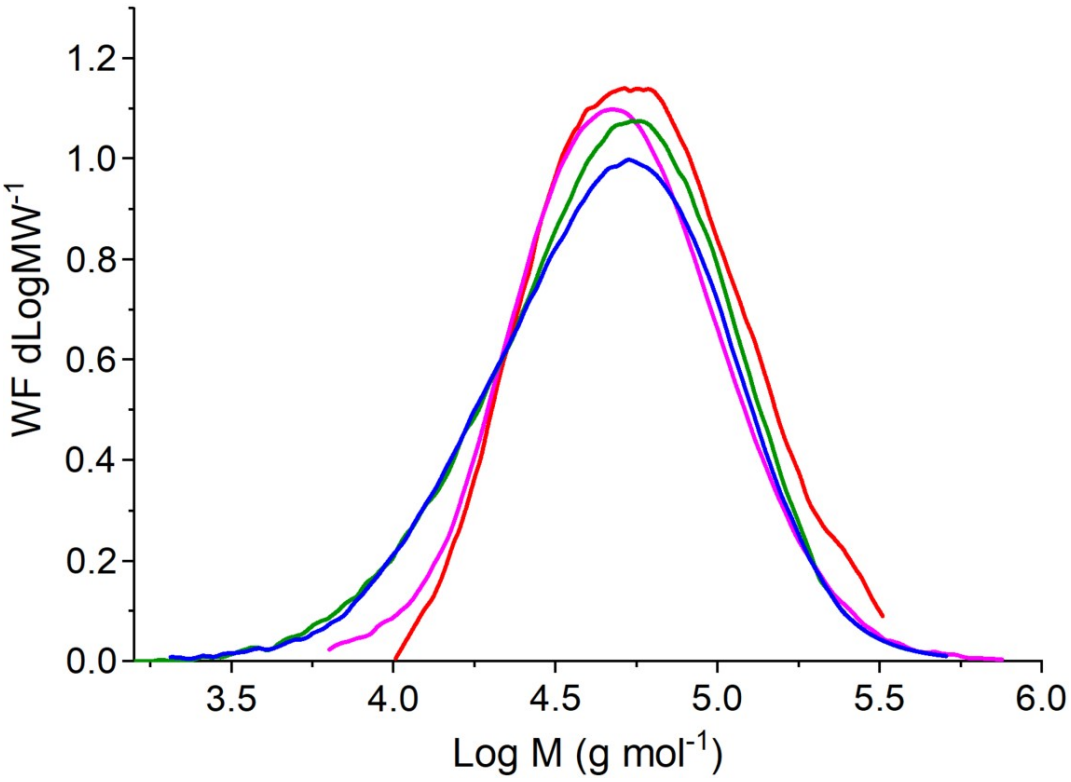

Figure S19. SEC chromatograms of the PBTTT-^{11}O, PBTTT-^{8}O, PBTTT-^{5}O, PBTTT-^{3}O, respectively

ThermoGravimetric Analysis (TGA)

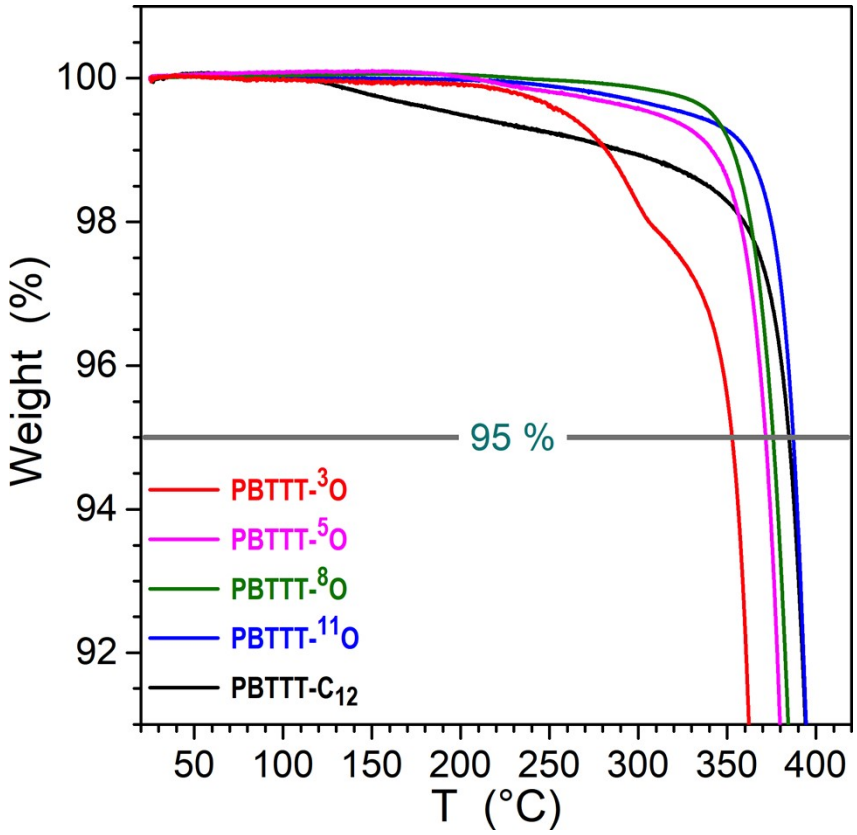

Figure S20. TGA curves of PBTTT-C_{12}, PBTTT-^{11}O, PBTTT-^{8}O, PBTTT-^{5}O, PBTTT-^{3}O, respectively.

PhotoElectron Spectroscopy in Air (PESA)

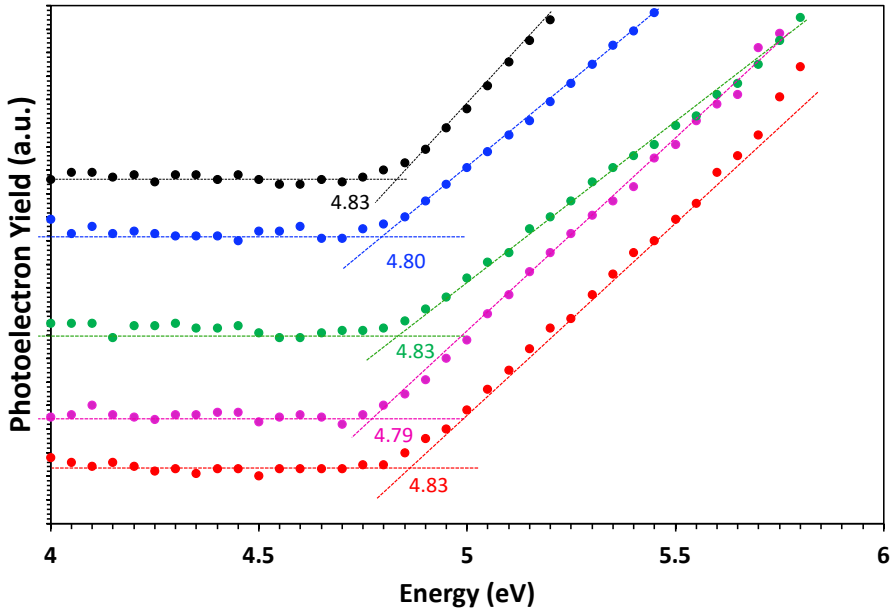

Figure S21. Photoelectron spectroscopy in air (PESA) spectra of PBTTT-C_{12}, PBTTT-^{11}O, PBTTT-^{8}O, PBTTT-^{5}O, PBTTT-^{3}O, respectively.

Cyclic Voltammetry (CV)

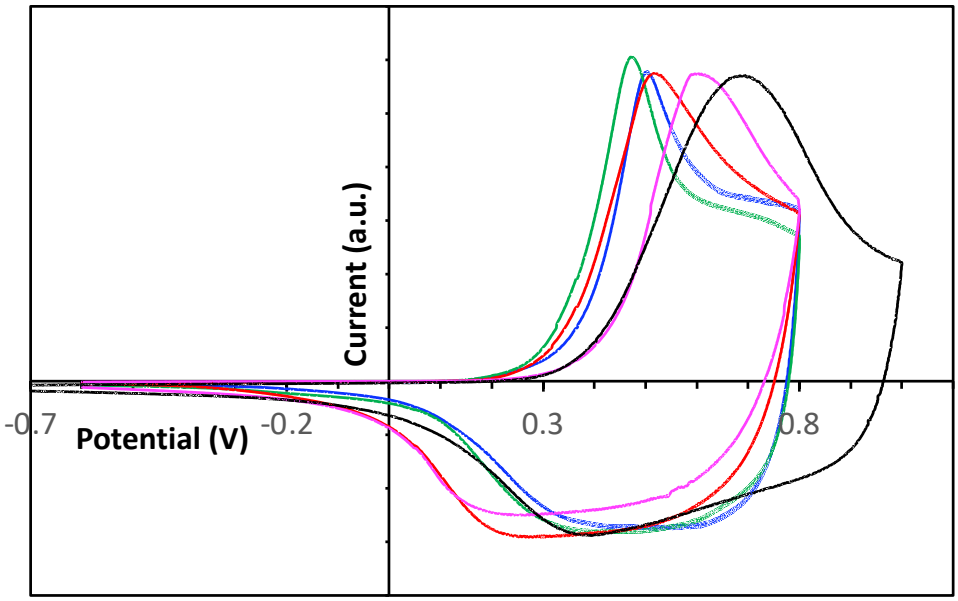

Figure S22. Cyclic voltamperograms of PBTTT-C_{12}, PBTTT-^{11}O, PBTTT-^{8}O, PBTTT-^{5}O, PBTTT-^{3}O, respectively (0.1 M Bu_4NPF_6/MeCN , scan rate 100 mV.s^{-1}).

N.B. *Slight differences in apparent oxidation potentials when scanned at a constant 100 mV* s^{-1}*, are observed by CV. The deeper HOMO levels found by CV compared to PESA suggest that the scan rate chosen was too fast to reach steady states and that CV results are driven by ion-diffusion limitations. The apparent higher HOMO for PBTTT-*^{3}*O, -*^{5}*O and -*^{8}*O compared to PBTTT-*^{11}*O and -*C_{12} *suggest that an oxygen closer to the backbone facilitate faster solvated ion uptake in the bulk polymer film due to favorable dipolar interactions between the ether function and the ions.*[S5,S6]

Energy level table

Table S1. Ionization potentials measured by CV and PESA of the synthesized PBTTTs.

	IP_{CV} (eV)	IP_{PESA} (eV)
PBTTT-C_{12}	5.1	4.8
PBTTT-^{11}O	5.1	4.8
PBTTT-^{8}O	5.0	4.8
PBTTT-^{5}O	5.0	4.8
PBTTT-^{3}O	5.0	4.8

UV-Visible absorbance spectroscopy

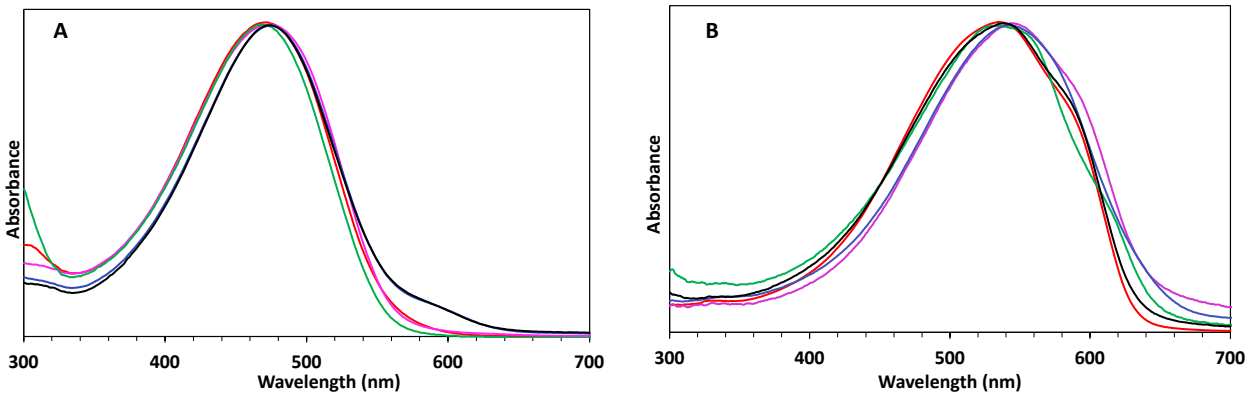

Figure S23. A. UV-visible absorbance spectra in chlorobenzene solutions at room temperature; **B.** UV-visible absorbance spectra in thin films of PBTTT-C_{12}, PBTTT-^{11}O, PBTTT-^{8}O, PBTTT-^{5}O, PBTTT-^{3}O, respectively.

Fast Scanning Calorimetry

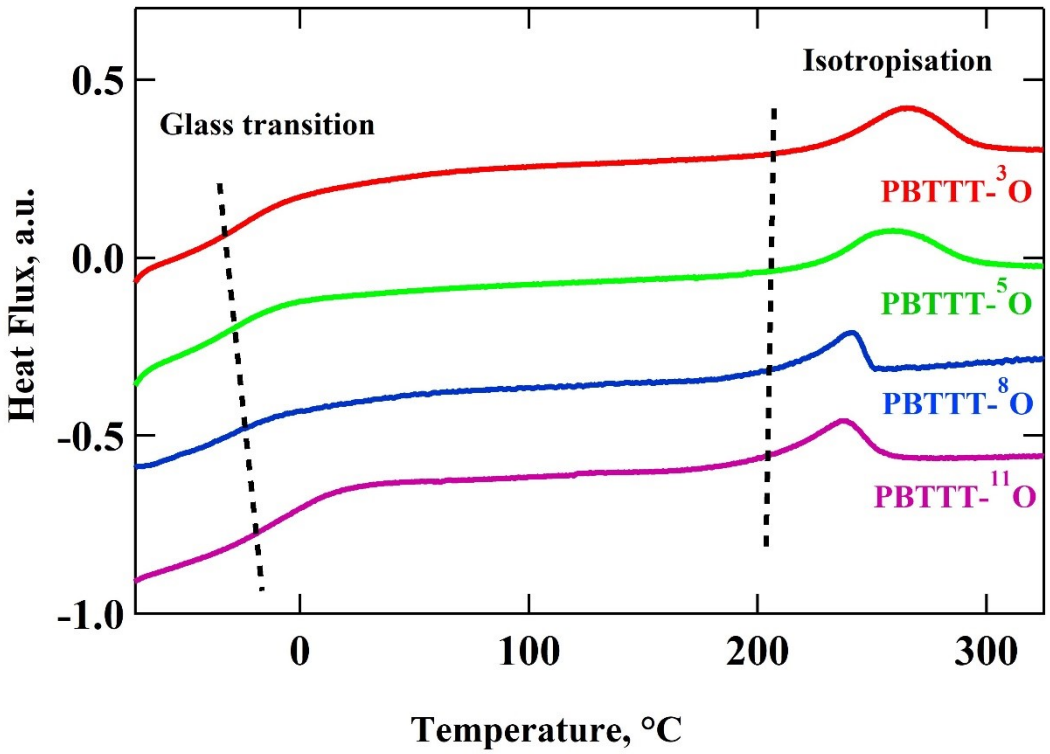

Figure S24. Fast scanning calorimeter heating traces recorded at a heating rate of 1000 ºC/s. The samples were previously quenched from the melt to -90 ºC at a rate of 1000 ºC/s. The dashed lines show the glass transition region and the onset of the isotropisation transition.

Small-Angle X-ray Scattering (SAXS)

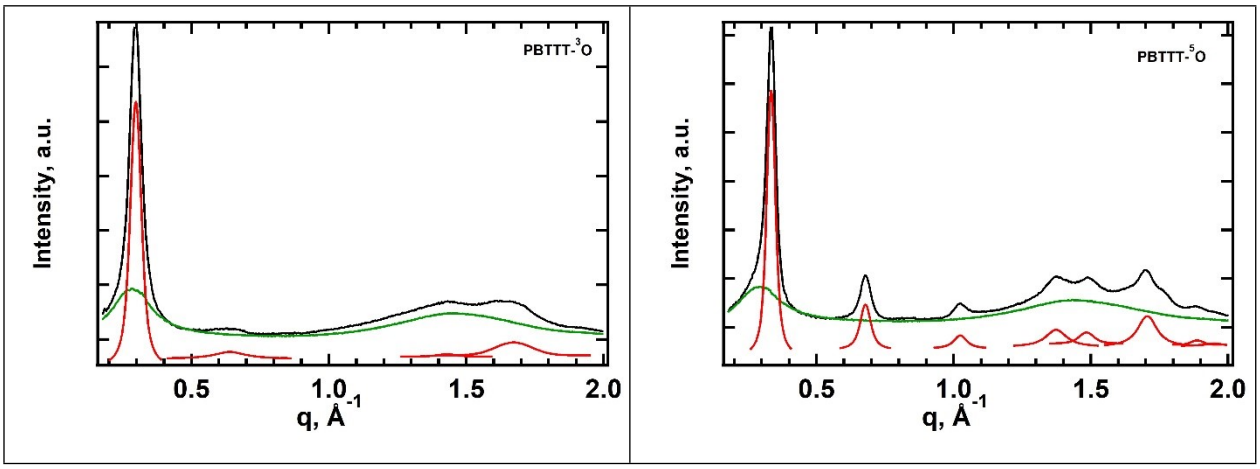

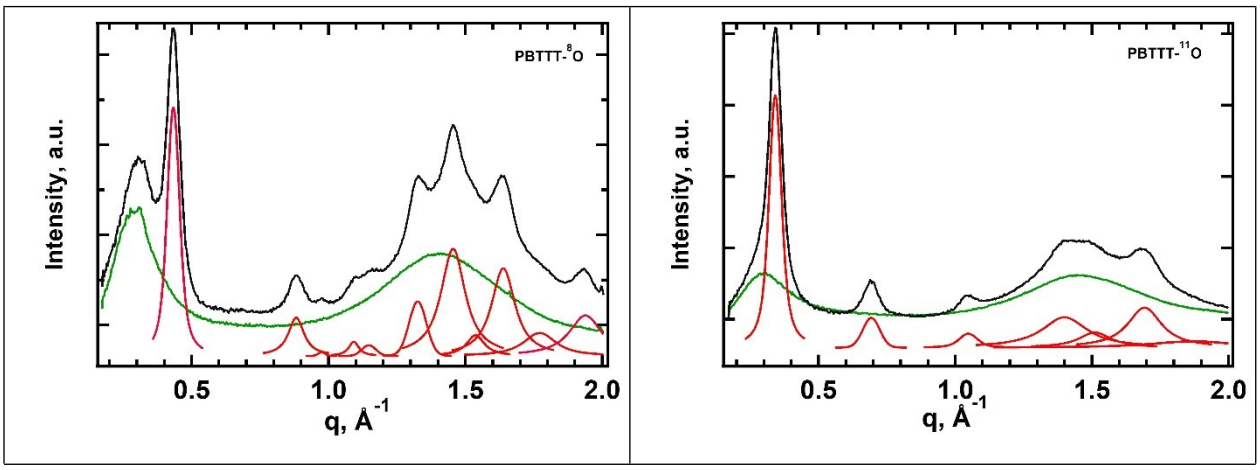

Figure S25. Decomposition of the room-temperature micro-focus X-ray scattering patterns (black curves) into a sum of crystalline peaks intensity (red curves) and amorphous halo (green curves). The shape of the amorphous halo was measured for each sample above the isotropisation temperature.

Temperature-dependent anisotropy

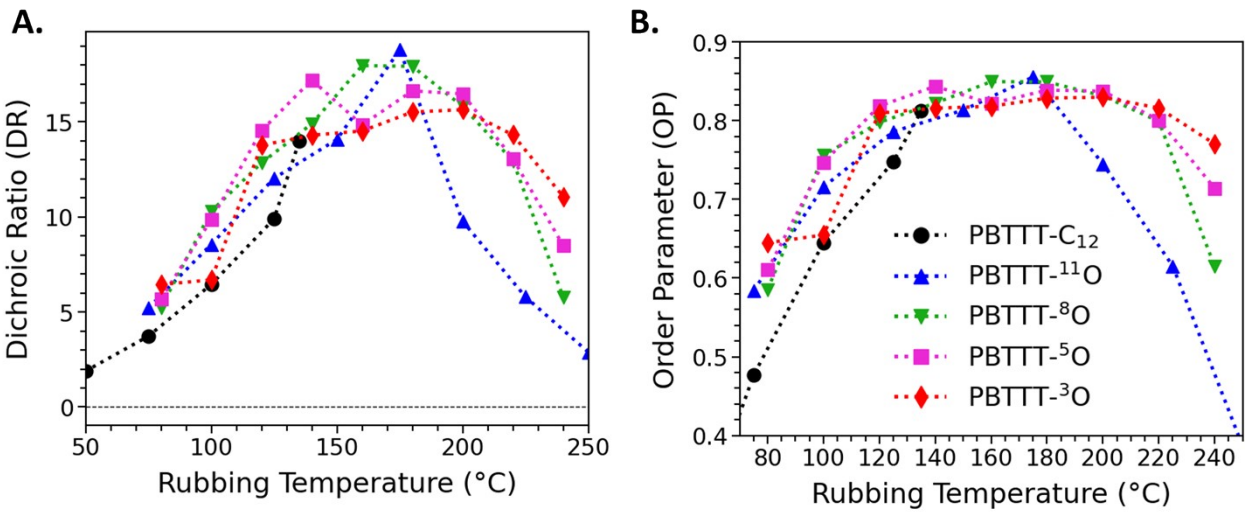

Figure S26. Evolution of the dichroic ratio ($DR = \frac{Abs//}{Abs_{\perp}}$) and the 3D order parameter ($OP = \frac{DR - 1}{DR + 2}$) for each polymer as a function of the rubbing temperature.

Polarized UV-Vis-NIR absorbance spectroscopy on F_6TCNNQ-doped films

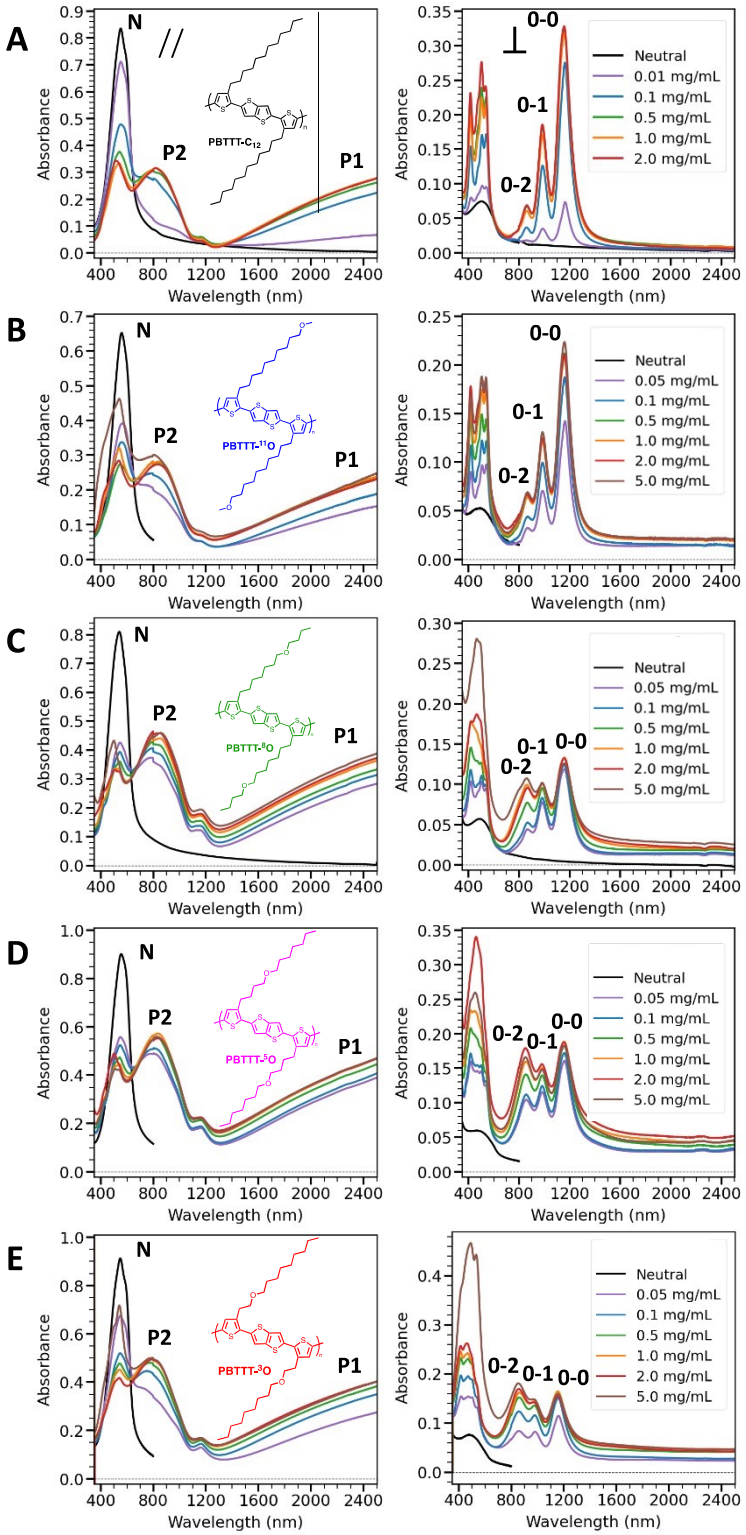

Figure S27. Polarized UV-vis-NIR absorbance spectra of oriented thin films of PBTTT-C_{12} and PBTTT-^{x}O doped with F_6TCNNQ in acetonitrile at various dopant concentrations. **A.** PBTTT-C_{12}, **B.** PBTTT-^{11}O, **C.** PBTTT-^{8}O, **D.** PBTTT-^{5}O, **E.** PBTTT-^{3}O. The light is polarized parallel (left) and perpendicular (right) to the rubbing direction. On the left, the spectra are mainly polymer signatures. On the right, the spectra are mainly dopant signatures. The main absorbance polaronic bands (P1 and P2), neutral polymer (N) and of the F_6TCNNQ radical mono/dianion are highlighted.

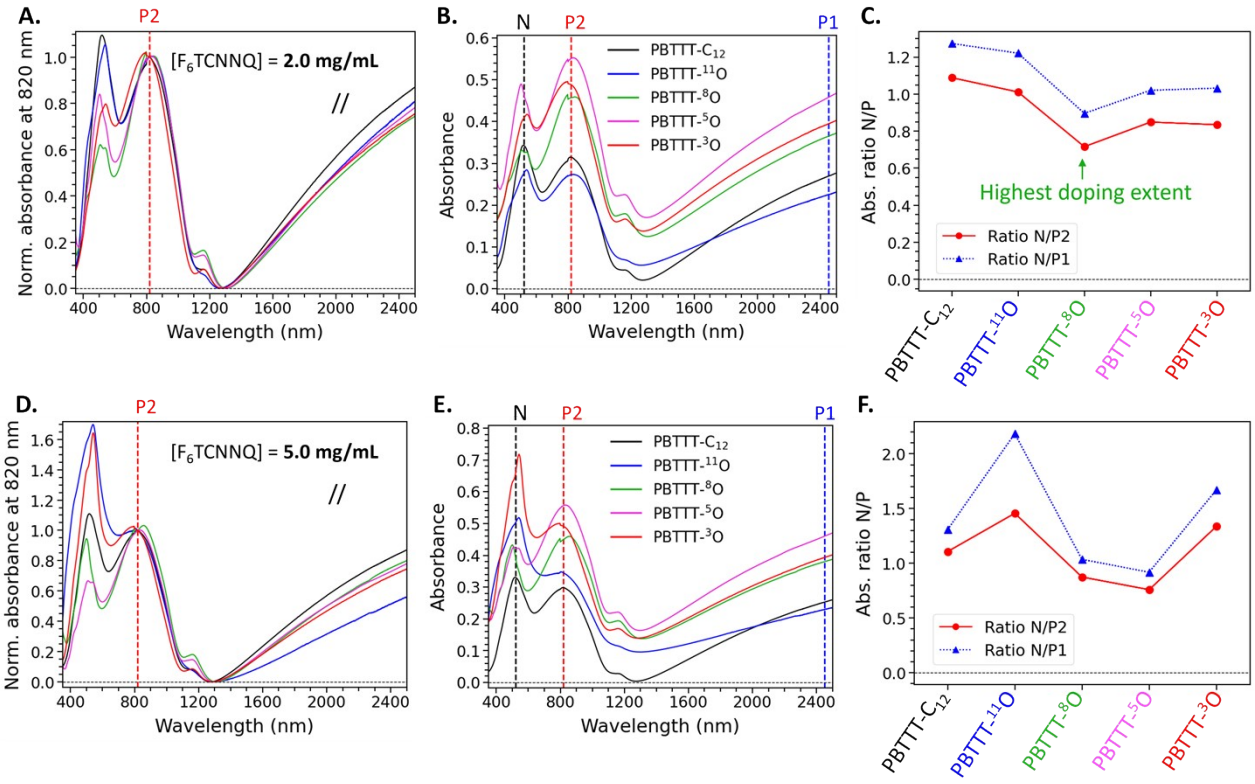

Figure S28. Overlaid for comparison purposes of UV-vis-NIR absorbance spectra of oriented thin films with light polarized parallel to the rubbing direction for all polymers at a given concentration of F_6TCNNQ. **A.B.C.** 2 mg.mL^{-1}, **D.E.F.** 5 mg.mL^{-1}. **A.D.** Absorbance spectra normalized by the maximum intensity at 820 nm (center of the polaronic P2 band). **B.E.** Corresponding raw data. **C.F.** Comparison of the doping extent by the ratio of the absorbance of the neutral band (N, 520 nm) over the maximum absorbance of the (bi)polaronic bands P2 (830 nm) and P1 (2450 nm). The

lower the N/P ratio, the higher the doping extent. This single wavelength analysis shows that PBTTT-^{8}O exhibits high doping extent for both 2 and 5 mg.mL^{-1}, in accordance with the high electrical conductivity found.

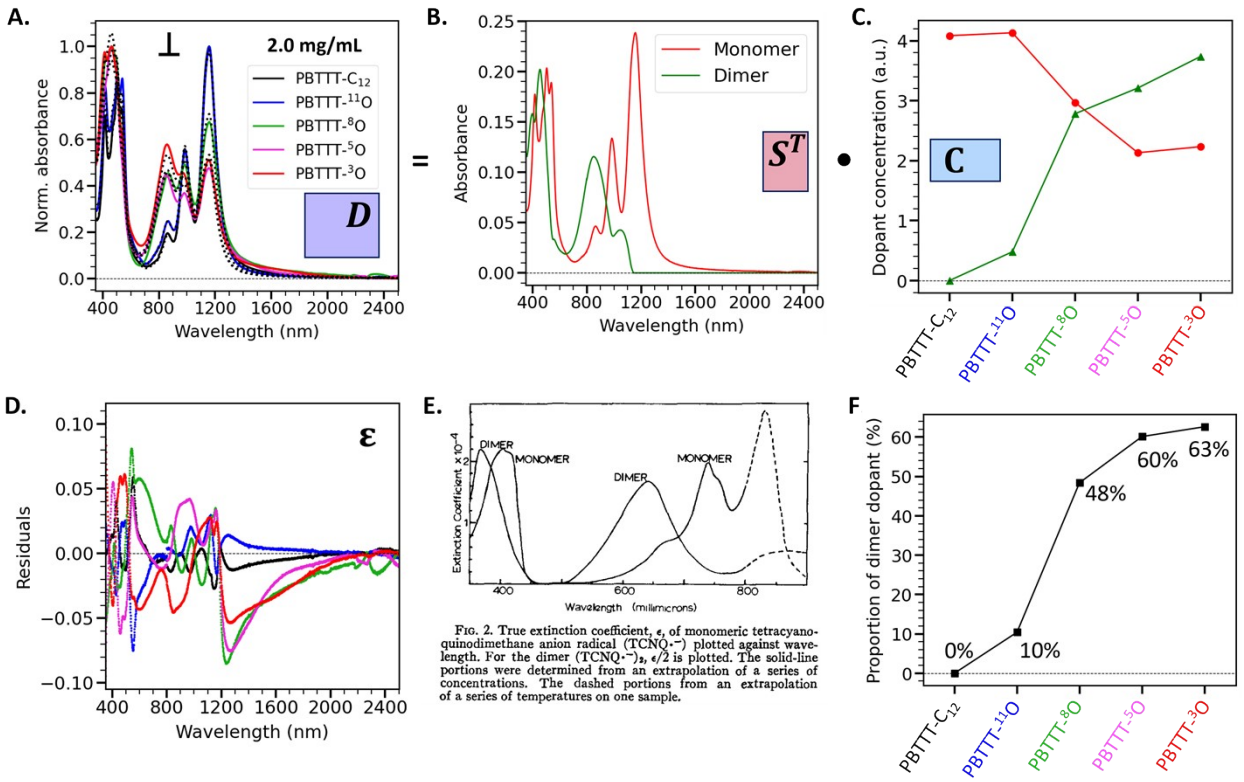

FIG. 2. True extinction coefficient, ϵ, of monomeric tetracyanoquinodimethane anion radical ($TCNQ\cdot^-$) plotted against wavelength. For the dimer $(TCNQ\cdot^-)_2$, $\epsilon/2$ is plotted. The solid-line portions were determined from an extrapolation of a series of concentrations. The dashed portions from an extrapolation of a series of temperatures on one sample.

Figure S29. MCR deconvolution of the normalized UV-vis-NIR absorbance spectra of oriented thin films with light polarized perpendicular to the rubbing direction when doped at 2 mg.mL^{-1}. The 3D matrix D (wavelength vs absorbance vs polymer) is computationally decomposed on an array of spectral signature (S) and an array of concentration for each polymer (C) following $D = S^T \cdot C + \varepsilon$, with ε the residual of the deconvolution, using the Python pyMCR package.[S7] **A.** Colored solid lines = normalized absorbance data, black dashed line = reconstructed data achieved by MCR. **B.** Spectral signature (S) found, showing that the data can be reasonably well fitted with only two distinct species with overlapping spectra. **C.** Resulting concentrations (C) of both species found for each polymer. The red curve is assigned to monomer of $F_6TCNNQ^{\bullet-}$ radical anion, and the green curve is assigned to $(F_6TCNNQ^{\bullet-})_2$ dimer. **D.** Residual (= difference between input data and MCR reconstructed data). **E.** Figure and caption reproduced from reference S8 to support the assignation of the species found to both monomer and dimer of the dopant. **F.**

Proportion of dimer dopant in percentage (*i.e.* ratio dimer/monomer) found for each polymer, highlighting that PBTTT-^{8}O exhibits equilibrated amounts of monomers and dimers (about 50/50%).

N.B. *Note that the highest electrical conductivity is reached for 5 mg.mL^{-1} but the UV-vis-NIR spectra at this concentration shows more than two species, being likely a complex mixture of neutral un-reacted dopants, monomer anions, dimers, and higher doping states. The 2 mg.mL^{-1} is hence selected for clarity.*

Transmission Electronic Microscopy (TEM) and Electronic Diffraction (ED)

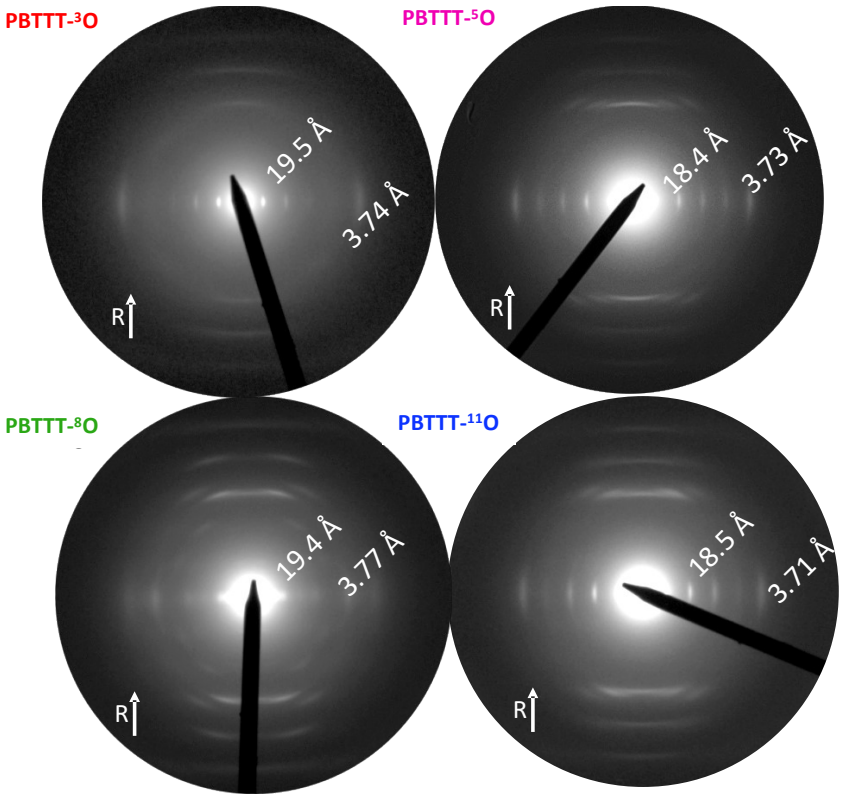

Figure S30. ED pattern of oriented PBTTT-^{x}O films. All films were oriented by rubbing at T_R in the 160 °C-170 °C range. Note the very different pattern for PBTTT-^{8}O compared to other PBTTT-^{x}O. For PBTTT-^{8}O the structure of the films is a mixture of two phases: (i) a liquid crystalline phase, characterized by d_{100} = 19.5 Å, and (ii) a monoclinic crystalline phase, with d_{100}=14.6 Å (red arrow

pointing at the reflection). The rubbing direction is vertical for all patterns as indicated by the upward white “R” arrow.

Variation of lattice parameter with respect to doping

We followed the evolution of the interlamellar distance of our PBTTT series during doping by low dose TEM. For PBTTT-C_{12}, we previously described a gradual increase of the lamellar distance with the dopant concentration solution (Figure S30). This feature is ascribed to the dopant intercalation within the side-chain region which increases the "pressure" and repels the lamella on both sidesAs the lamellae are oriented face-on on the substrate, the π-stacking distance is not measurable by TEM.

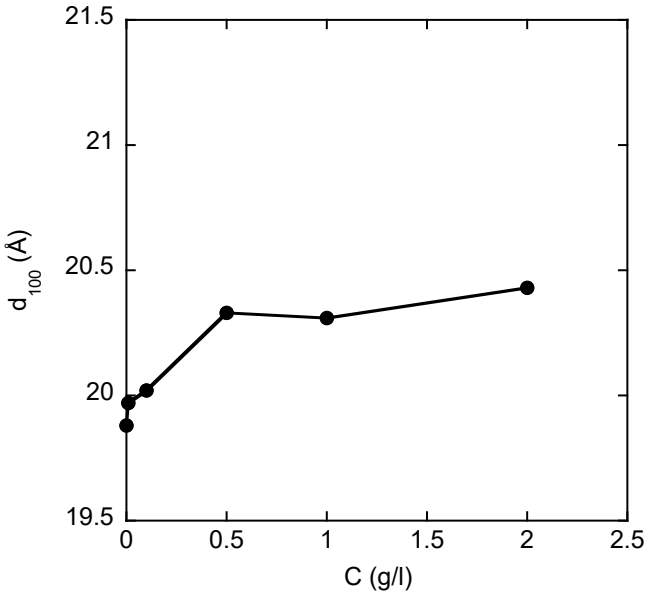

Figure S31. Interlamellar distance as function of F_6TCNNQ doping concentration for oriented PBTTT- C_{12} (T_R=125°C). The films being mainly face-on oriented, the d_{020} could not be measured.

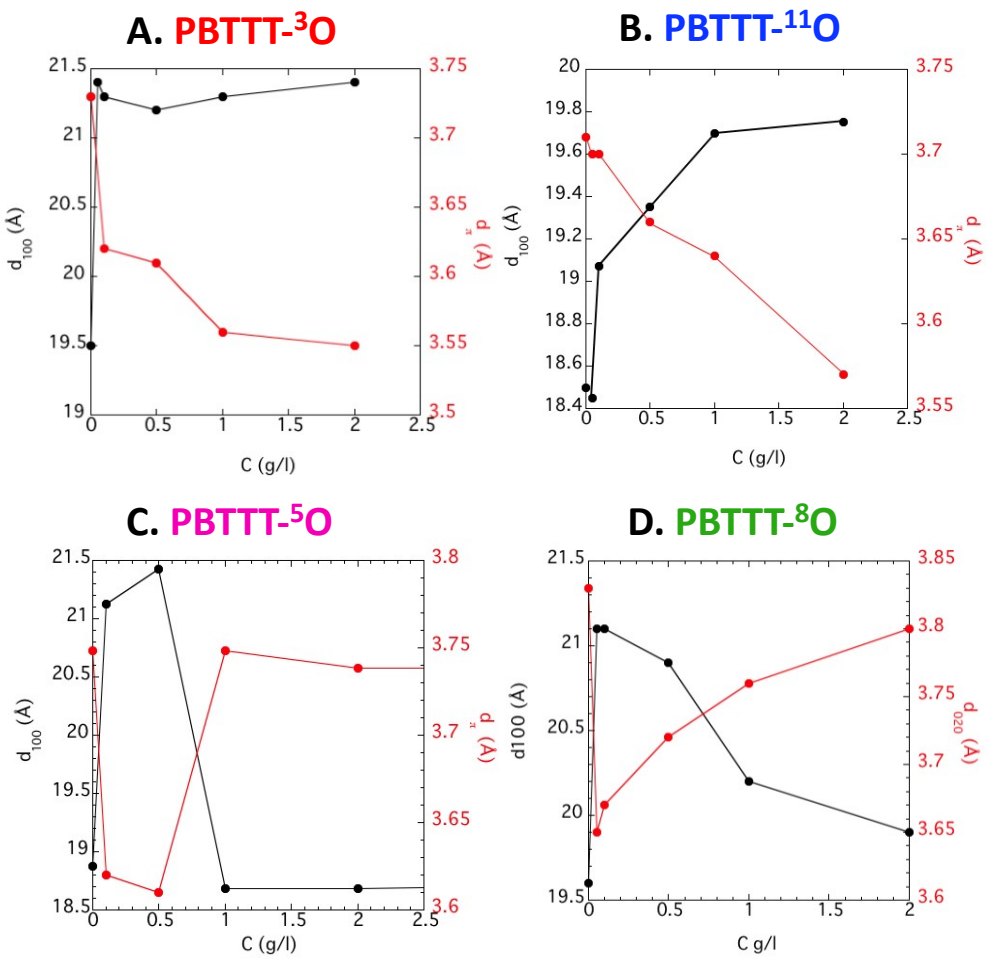

Figure S32. Interlamellar distances as function of F_6TCNNQ doping concentration for **A.** PBTTT-^{3}O, **B.** PBTTT-^{11}O, **C.** PBTTT-^{5}O and **D.** PBTTT-^{8}O.

For PBTTT-^{3}O and PBTTT^{11}O the situation is similar with an increase of the interlamellar distance as the concentration of the doping solution increase (Figures S32A and S32B). This likely reflects the increase in dopant concentration in the side chain region. However, for PBTTT-^{5}O and PBTTT-^{8}O, the situation is completely different (Figures S32C and S32D). At low doping concentrations (< 0.5 mg.mL^{-1}) the interlamellar distance increases brutally (from 19 Å to 21 Å), reflecting dopant incorporation in the side chains. And at higher doping concentrations (> 0.5 mg.mL^{-1}), the interlamellar distances almost recover to their values in the pristine undoped state (19 Å).

Thermoelectric performance

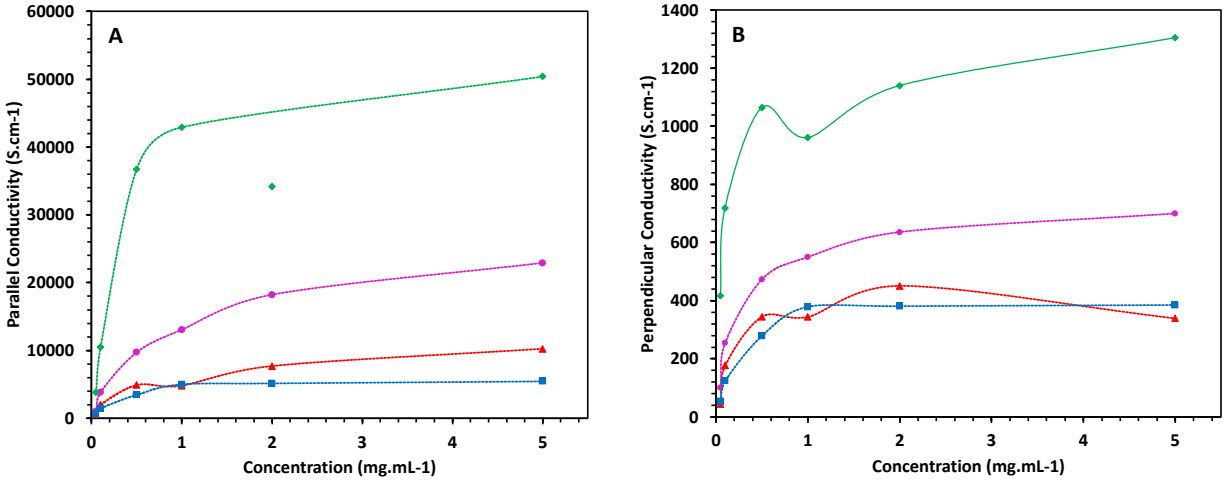

Figure S33. Electrical conductivity measured for PBTTT-^{3}O, PBTTT-^{5}O, PBTTT-^{8}O and PBTTT-^{11}O, **A.** in parallel direction to the rubbing, **B.** in perpendicular direction to the rubbing, as a function of the dopant concentration.

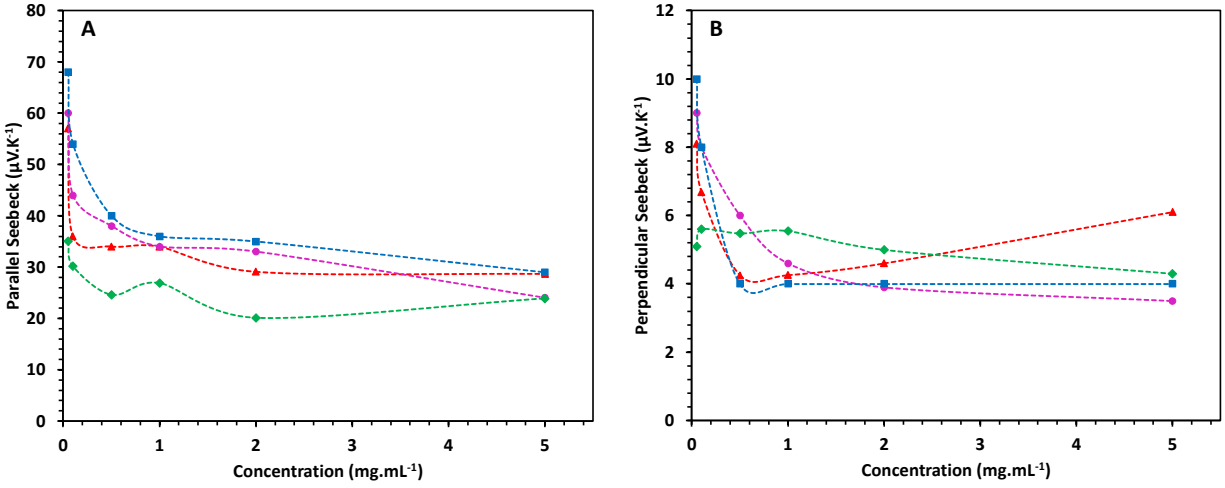

Figure S34. Seebeck coefficient measured for PBTTT-^{3}O, PBTTT-^{5}O, PBTTT-^{8}O and PBTTT-^{11}O, **A.** in parallel direction to the rubbing, **B.** in perpendicular direction to the rubbing, as a function of the dopant concentration.

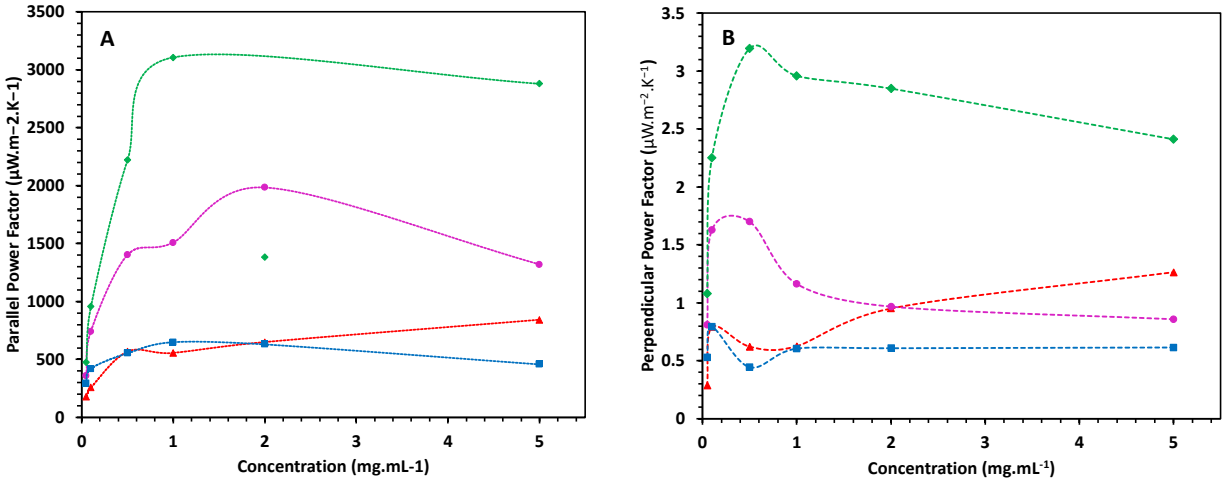

Figure S35. Power factors measured for PBTTT-^{3}O, PBTTT-^{5}O, PBTTT-^{8}O and PBTTT-^{11}O, **A.** in parallel direction to the rubbing, **B.** in perpendicular direction to the rubbing, as a function of the dopant concentration.

N.B. *The anisotropy, previously highlighted through the dichroic ratio calculations, is perfectly reflected in the TE measurements performed perpendicular to the rubbing direction. Indeed, despite, the perpendicular TE parameters follow exactly the same trend than in parallel, they are all significantly reduced as compared to parallel ones. As illustration, electrical conductivities decreased according to the following order: PBTTT-^{8}O, still the highest (1200 S.cm^{-1}) > PBTTT-^{5}O (650 S.cm^{-1}) > PBTTT-^{11}/^{3}O/C_{12} (in the 200-400 S.cm^{-1} range).* `

Table S2. Summary of some of the best reported Organic Thermoelectric Materials

Polymer	S (µVK^{-1})	σ (S cm^{-1})	PF (µWm^{-1} K^{-2})	Ref
Non-aligned (isotropic)				
PA	28.4	11110	900	S9
PEDOT-Tos-PP	117	923	1270	S10
PDPP-$g_3$2$T_{0.3}$	56	360	110	S11
DPP-BTz	49	495	123	S12
P3EOPT	34	250	12.5	S13

PBTTT-C_{14}	42	180	135	S14
Aligned (anisotropic)				
PBTTT-C_{12}	17	4345	137	S15
P3HT	56	509	160	S16
PBTTT-^{5}O	24	20000	1320	**This work**
PBTTT-^{8}O	24	50000	2900	**This work**

References

[S1] V. Untilova, T. Biskup, L. Biniek, V. Vijayakumar, M. Brinkmann, *Macromolecules* **2020**, *53*, 2441.

[S2] V. Vijayakumar, P. Durand, H. Zeng, V. Untilova, L. Herrmann, P. Algayer, N. Leclerc, M. Brinkmann, *J. Mater. Chem. C* **2020**, *8*, 16470.

[S3] A. Hamidi-sakr, L. Biniek, J.-L. Bantignies, D. Maurin, L. Herrmann, N. Leclerc, P. Lévêque, V. Vijayakumar, N. Zimmermann, M. Brinkmann, *Adv. Funct. Mater*. **2017**, *27*, 1700173.

[S4] V. Vijayakumar, E. Zaborova, L. Biniek, H. Zeng, L. Herrmann, A. Carvalho, O. Boyron, N. Leclerc, M. Brinkmann, *ACS Appl. Mater. Interfaces* **2019**, *11*, 4942.

[S5] A. Giovannitti, I. P. Maria, D. Hanifi, M. J. Donahue, D. Bryant, K. J. Barth, B. E. Makdah, A. Savva, D. Moia, M. Zetek, P. R. F. Barnes, O. G. Reid, S. Inal, G. Rumbles, G. G. Malliaras, J. Nelson, J. Rivnay, I. McCulloch, *Chem. Mater*. **2018**, *30*, 2945.

[S6] P. Durand, H. Zeng, T. Biskup, V. Vijayakumar, V. Untilova, C. Kiefer, B. Heinrich, L. Herrmann, M. Brinkmann, N. Leclerc, *Adv. Energy Mater.* **2022**, *12*, 2103049.

[S7] C. H. Camp, *J. Res. Natl. Inst. Stand. Technol.* **2019**, *124*, 124018.

[S8] R. H. Boyd, W. D. Phillips, *J. Chem. Phys.* **1965**, *43*, 2927–2929.

[S9] Y. W. Park, *Synth. Met.* **1991**, 45, 173.

[S10] T. Park, C. Park, B. Kim, H. Shin, E. Kim, *Energy Environ. Sci.* **2013**, 6, 788.

[S11] H. Li, J. Song, J. Xiao, L. Wu, H. E. Katz, L. Chen, *Adv. Funct. Mater.*, **2020**, 30, 2004378.

[S12] D. Wang, J. Ding, X. Dai, L. Xiang, D. Ye, Z. He, F. Zhang, S.-H. Jung, J.-K. Lee, C.-A. Di, D. Zhu, *Adv. Mater.* **2022**, 2208215.

[S13] L. Chen, W. Liu, Y. Yan, X. Su, S. Xiao, X. Lu, C. Uherc, X. Tang, *J. Mater. Chem. C* **2019**, 7, 2333-2344.

[S14] J. Kim, D. Ju, S. Kim, K. Cho, *Adv. Funct. Mater.* **2024**, 34, 2309156.

[S15] Y. Huang, D. H. L. The, I. E. Jacobs, X. Jiao, Q. He, M. Statz, X. Ren, X. Huang, I. McCulloch, M. Heeney, C. McNeill, H. Sirringhaus, *Appl. Phys. Lett.* **2021**, 119, 111903.

[S16] V. Untilova, J. Hynynen, A. I. Hofmann, D. Scheunemann, Y. Zhang, S. Barlow, M. Kemerink, S. R. Marder, L. Biniek, C. Müller, M. Brinkmann, *Macromolecules,* **2020**, 53, 6314.